Nonlinear waves in granular crystals

Antoine Levitt

Hertford College
University of Oxford

A thesis submitted for the degree of *Master of Science in Mathematical Modelling and Scientific Computing* 2009–2010

Abstract

We investigate excitations in one-dimensional granular crystals, *i.e.* chains of solid beads with nonlinear interaction forces. These chains have attracted attention because of their relative experimental simplicity and interesting dynamics. They can be modelled as chains of coupled oscillators in a model reminiscent of the celebrated Fermi-Pasta-Ulam (FPU) equations. The nonlinearity of the interaction leads to complex behaviour, including solitary waves and discrete breathers—periodic oscillations that are localised in space. We review the theory of granular chains starting from the contact law between two spheres and then consider some mathematical and numerical aspects of discrete breathers. We try to link some features of wave scattering by discrete breathers to Fano resonances, a resonant suppression of transmission observed in several other physical systems.

Acknowledgments

Thanks to Mason Porter for his guidance throughout this project, to Felix Flicker for explaining his MPhys work to me, and to Nicholas Boechler and Georgios Theocharis for initial breather data and useful discussions.

Note: Parts of the introductory Section 2—namely 2.1, 2.2 and 2.4— include modified excerpts from my special topic submitted for the course Nonlinear Systems in Hilary Term 2010.

Contents

1 Introduction

This dissertation is concerned with excitations in Hamiltonian lattices. Such lattices can be thought of as chains of interacting oscillators. An example of such a chain is the class of Fermi-Pasta-Ulam (FPU) lattices. In these models, each oscillator u_n interacts with its nearest neighbours according to the second-order differential equation

$$\ddot{u}_n = W'(u_{n+1} - u_n) - W'(u_n - u_{n-1}), \tag{1.1}$$

where W is the interaction potential. This can be seen as a nonlinear generalisation of systems of masses connected by springs. This model dates back to the famous FPU experiment [13] and has been extensively studied for its interesting dynamics and connections to soliton theory [35].

The discreteness of the system (1.1) means that infinitesimal waves of arbitrary spatial frequencies cannot propagate, and there is a corresponding upper bound on the temporal frequencies the chain supports. This property allows nonlinear oscillations to avoid resonances with small-amplitude waves, and localised oscillations can persist without radiating energy. These localised excitations are called discrete breathers (DBs) or intrinsic localised modes (ILMs) because they arise in a spatially homogeneous system (where there are no differences between sites), and are caused by the dynamics only and not by impurities in the chain. Their relatively counter-intuitive character, wide applicability, and strong stability properties make them an important subject of research in nonlinear science [16].

Such discrete breathers, first touched on in 1969 [34], were studied in greater detail in the 1990s, both theoretically and experimentally. Recently, there have been numerical and experimental reports of discrete breathers in chains of alternating spherical metal beads [3, 39]. When two beads are pressed against each other, they repel and this leads to an equation of the form (1.1), with an interaction potential dictated by the Hertz contact law

$$W'(x) \propto \begin{cases} x^{3/2} & \text{when } x > 0, \\ 0 & \text{when } x \leq 0, \end{cases} \tag{1.2}$$

where x is the overlap between two adjacent spheres.

While discrete breathers have been extensively studied in certain systems, some properties are still incompletely understood. In particular, the first step to understand the effect of a discrete breather on its surroundings is to study the problem of wave scattering: What happens if we send a small-amplitude wave towards the breather? If the breather is stable, the incoming wave will not have any significant effect on the localised oscillations. However, the interaction with the breather will generate reflected and transmitted waves, sometimes with different frequencies. A peculiar effect where a perfect reflection (no transmitted wave) occurs for some frequency was theoretically and numerically observed for a class of systems similar to the granular chain. This perfect reflection was linked to Fano resonances, a phenomenon found to play an important role in many branches of physics [29], and in particular were introduced to study interaction of light with matter. This effect is well understood for linear and weakly nonlinear systems, but highly nonlinear ones such that the one we are considering

still pose a challenge because of the inapplicability of perturbation methods. An objective of this work is to study the possibility of Fano resonances in the granular chain.

This report is organised as follows. First, we present our system of study and the equations of motions for a chain of spherical solid beads, and investigate some of the properties of this lattice. Then, we focus on discrete breathers, beginning with a general study then examining their existence and computational aspects in our system. After introducing at the phenomenon of Fano resonances on progressively more complex examples, we examine wave scattering by discrete breathers in the granular chain, recall results of Fano resonances for discrete breathers and try to observe Fano resonances in granular chains. Our conclusion conjectures the nonexistence of such resonances in the granular chain, and highlights issues in their observation for systems where they are known to exist.

2 The Hertzian Chain

The main object of our study is a chain of solid spheres. These solid spheres, when pressed against each other, deform slightly and exert a repelling force, pushing them apart. This repelling force is responsible for interesting dynamics, due to its nonlinearity.

2.1 The Hertzian Contact

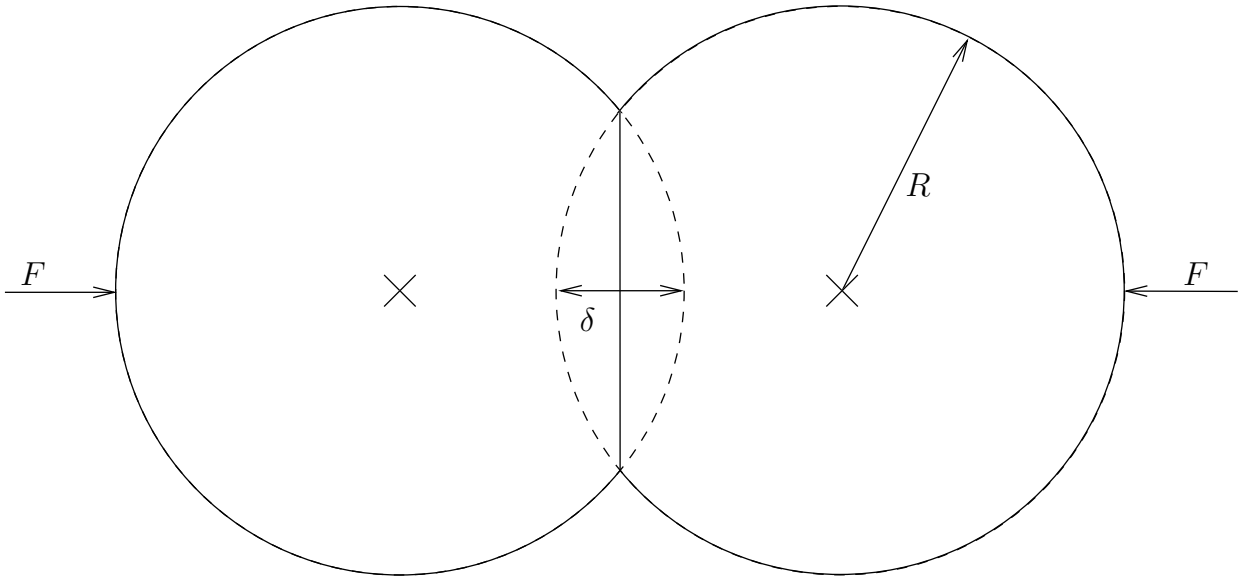

Figure 2.1: Contact force between two grains.

We consider the situation sketched in Figure 2.1. We assume two perfectly identical spherical bodies of radius R, pressed against each other with overlap δ. In this configuration, spheres deform, and the resulting tendency of the materials to regain their original shape produces a repelling force. For small deformations and sufficiently stiff materials, this is a problem in

linear elasticity. Its exact solution is known as Hertz's Law and is given by (derived in [23], reproduced in Reference [8])

$$F = A\delta^{3/2}, \text{ with } A = \frac{E\sqrt{2R}}{3(1-\nu^2)}. \tag{2.1}$$

Here, ν is Poisson's ratio, and E is Young's modulus, both characteristics of the material used. Young's modulus E measures the stiffness of the material to deformations (the same way that a spring constant measures the stiffness of a simple spring) and Poisson's ratio ν measures the tendency of the material to expand in other directions when compressed.

Equation (2.1) simply means that the force felt by two grains with overlap δ due to their deformation is proportional to $\delta^{3/2}$. The exponent in this formula depends on the contact geometry. For instance, a contact between cubes would yield a contact force proportional to δ, and a contact in presence of conical asperities yields a force proportional to δ^2 [20].

When δ is varying in time, Hertz's Law is still valid provided the variation is slow enough for the material to always assume its equilibrium state. In other words, the formula is valid as long as the speed of the waves in the chain is negligible compared to the speed of wave propagation (speed of sound) in the material of the beads. This is a "quasistatic" approximation, also encountered in other domains of physics (for instance, thermodynamics or electrodynamics). This approximation is satisfactory for typical experimental setups [11], and we will assume it is the case in our study.

2.2 The Hertzian Chain

Now, we consider a chain of grains. The setup is represented Figure 2.2. Each interior grain may have an overlap with its two neighbours and be subjected to corresponding forces. We will consider an infinite chain when obtaining analytical results, and we will use a finite one for the numerical experiments, together with appropriate boundary conditions. Throughout this report, we use the open boundary conditions $u_0 = u_1, u_{N+1} = u_N$ for a chain of N oscillators $u_1 \dots u_N$. These boundary conditions are also called "free" because the position of the oscillator at the end is not constrained. They correspond to Neumann boundary conditions for a partial differential equation.

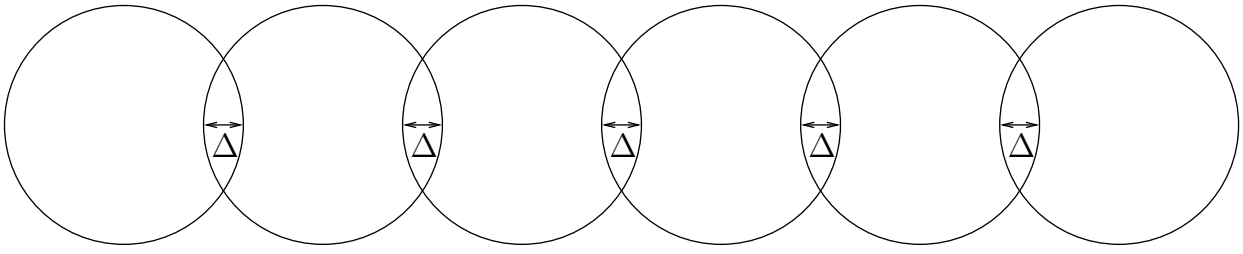

Figure 2.2: Horizontal chain of grains at equilibrium.

We assume that our system is precompressed by an amount Δ: in an experimental setup, forces are exerted at both ends so that, at equilibrium, the overlap between adjacent grains

is Δ. We denote by u_n the displacement of grain n from its equilibrium position. The force exerted by grain $n+1$ on grain n is

$$\begin{aligned} F &= -A\delta_+^{3/2} \\ &= -A[\Delta - (u_{n+1} - u_n)]_+^{3/2}. \end{aligned}$$

Here the + subscript denotes the positive part: when $(\Delta - (u_{i+1} - u_i))$ is negative, the grains do not touch each other, and the force is zero.

The equation of motion for grain n of mass m, obtained by application of Newton's law, is then

$$m\ddot{u}_n = A\left[\Delta - (u_n - u_{n-1})\right]_+^{3/2} - A\left[\Delta - (u_{n+1} - u_n)\right]_+^{3/2}. \tag{2.2}$$

This equation is an example of a Fermi-Pasta-Ulam (FPU) system, which is an important class of system of coupled oscillators. These systems are extensively studied in nonlinear science for their intriguing wave propagation behaviour and connections to solitons [35].

This system is at equilibrium when all the displacements u_n are zero. Disturbances around this equilibrium will propagate. Of particular importance for the existence of breathers is the propagation of infinitesimally small disturbances, *i.e.* the dynamics in the linear regime.

2.3 Linear Spectrum

When considering small disturbances around an equilibrium, it is often instructive to analyse the linearised equations in order to gain insight about the behaviour of these disturbances. The form of (2.2)—a second order ordinary differential equation with nearest-neighbour coupling— is reminiscent of a wave equation, and suggests wave propagation. Indeed, when linearising (2.2) around the equilibrium $u_n = 0$, one obtains the coupled set of linear differential equations for the perturbations e_n at site n

$$\begin{aligned} m\ddot{e}_n &= K(e_{n+1} - 2e_n + e_{n-1}), \text{ where} \\ K &= \frac{3}{2}A\sqrt{\Delta} \end{aligned} \tag{2.3}$$

is the linear stiffness.

The term $e_{n+1} - 2e_n + e_{n-1}$ in this equation is the discrete analogue of the Laplacian operator, and this equation forms a discrete version of the classic linear wave equation $\frac{\partial^2 e}{\partial t^2} = c^2 \frac{\partial^2 e}{\partial x^2}$. Correspondingly, it should support propagating waves. To check that, we use the plane wave ansatz

$$e_n = e^{i(\omega t - qn)}$$

describing a wave propagating in the positive direction with frequency ω and wavenumber q. These linear waves are also called phonons, in reference to a similar concept in solid state physics.

Inserting this ansatz into the linearised equations (2.3) yields a *dispersion relation* which relates the temporal and spatial frequencies ω and q

$$\begin{aligned} -\omega^2 &= \frac{K}{m}(e^{-iq} - 2 + e^{iq}) \\ &= 2\frac{K}{m}(1 - \cos q) \\ \implies \omega &= \pm 2\sqrt{\frac{K}{m}}\sin(q/2). \end{aligned} \tag{2.4}$$

This equation encodes the properties of linear waves in the Hertzian chain:

- The wave velocity scales with the square root of the linear stiffness, and the inverse square root of the mass of the beads. That is not surprising and the scaling is similar to a linear string or a spring-mass system.
- The dispersion relation is nonlinear. This means that our system is *dispersive*: a wave packet cannot propagate through the chain without changing shape. A wave packet around frequency ω propagates at the *group velocity* $\frac{\mathrm{d}\omega}{\mathrm{d}q}$ which is different from the phase velocity $\frac{\omega}{q}$. This contrasts with the continuous wave equation, whose dispersion relation is linear, and which is non-dispersive.
- For small q, *i.e.* large wavelengths, our equation is well approximated using a continuum limit, and the dispersion relation can be approximated by $\omega = \sqrt{\frac{K}{M}}q$, implying that our system is weakly dispersive for large wavelengths.
- The spectrum has finite bandwidth: $\omega \in \left[0, 2\sqrt{\frac{K}{M}}\right]$. The chain, being discrete, cannot support arbitrarily high-frequency spatial oscillations, which are linked to high-frequency temporal oscillations. This is due to the discreteness of the lattice: a continuous wave equation such as $\frac{\partial^2 e}{\partial t^2} = c^2\frac{\partial^2 e}{\partial x^2}$ has an infinite bandwidth and allows arbitrarily fast oscillations. This feature of discrete systems will, as we shall see later, have the consequence that intrinsic localised modes (discrete breathers) can exist in our system, which is not generally the case in continuous ones.

2.4 Solitary Waves

Plane waves are found in the limit of small amplitudes, or high precompressions. In the opposite limit, we find solitary waves. Solitary waves are highly nonlinear waves that travel through the chain without changing shape [35].

Numerically, it is easy to generate an approximate solitary wave, simply by exciting a site with a high amplitude compared to the precompression Δ. For instance, Figure 2.3 represents a solitary wave at zero precompression obtained by simply imposing $\dot{u}_{100}(0) = 100$ with all other initial condition being equal to zero.

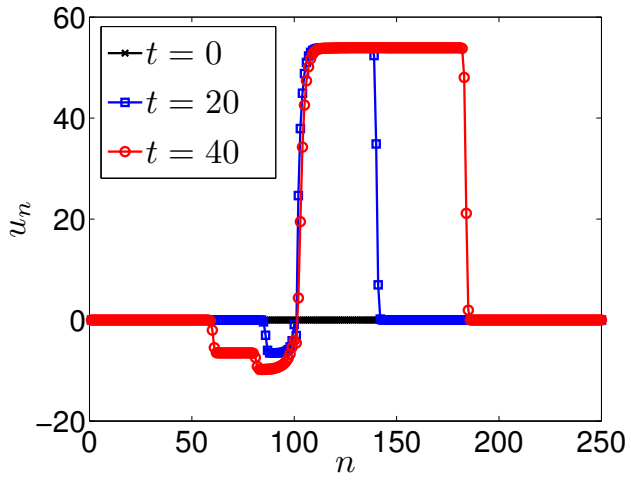

Figure 2.3: Solitary wave at zero precompression. The front moves to the right, leaving the lattice behind it compressed. Secondary solitary waves of smaller amplitude propagate to the left. We use a chain of size $N = 250$. The parameter values were $m = A = 1$ and $\Delta = 0$. Site $n = 100$ is excited at $t = 0$ with a velocity of 100.

Solitary waves in granular crystals have been studied analytically, beginning with the work of Nesterenko [32, 33], who found an approximate explicit form for solitary waves in a continuous limit. The derivation we present here is from the presentation by Chatterjee [6].

For simplicity, let us consider the case without any external precompression, that is, $\Delta = 0$. This is not necessary: the solitary wave phenomenon is not specific to this case, and can be found outside the linear range for nonzero precompression (see Reference [38] for the use of an existence proof for solitary waves with precompression, using a theorem of Friesecke and Wattis [19]). However, this simplified case allows for explicit calculations.

Rescaling the time as $t' = \sqrt{\frac{A}{m}}\, t$ allows us to nondimensionalise our equation of motion in the form

$$\ddot{u}_n = (u_{n-1} - u_n)_+^{3/2} - (u_n - u_{n+1})_+^{3/2}. \tag{2.5}$$

We will now look for solitary wave solutions of equation (2.5). We assume a decreasing wave front, that is, one for which $u_n \geq u_{n+1}$. Physically, this corresponds to having grains being compressed. This condition allows us to only consider interacting grains, which makes the analysis easier. We look for a travelling wave solution supported by an underlying smooth function u

$$u_n(t) = u(\xi) = u(t - bn), \tag{2.6}$$

where b is an arbitrary constant. This constant will serve as a bookkeeping parameter, which we can scale to 1 without loss of generality (by scaling ξ and t appropriately), and is used only to easily perform a Taylor series development of the equations of motion (2.5). The condition $u_n \geq u_{n+1}$ corresponds to requiring u to be nonincreasing.

We will use the long-wavelength approximation. This consists in considering a slow variation in the displacements : $u_n - u_{n+1} \ll u_n$. Under this hypothesis, it is reasonable to expand u_{n+1} and u_{n-1} in Taylor series

$$\begin{aligned} u_{n+1}(t) &= u(t - bn - b) \\ &= u(t - bn) - b\frac{\mathrm{d}u}{\mathrm{d}t}(t - bn) + \frac{b^2}{2}\frac{\mathrm{d}^2u}{\mathrm{d}t^2}(t - bn) + \mathcal{O}(b^3) \\ u_{n-1}(t) &= u(t - bn) + b\frac{\mathrm{d}u}{\mathrm{d}t}(t - bn) + \frac{b^2}{2}\frac{\mathrm{d}^2u}{\mathrm{d}t^2}(t - bn) + \mathcal{O}(b^3) \end{aligned}$$

Plugging these expansions into the equation of motion, and expanding in powers of b, we get

$$u_{\xi\xi} = \frac{3}{2}b^{5/2}\sqrt{u_\xi}u_{\xi\xi} + \frac{1}{8}b^{9/2}\left(\sqrt{u_\xi}u_{\xi\xi\xi\xi} + \frac{u_{\xi\xi}u_{\xi\xi\xi}}{\sqrt{u_\xi}} - \frac{1}{8}\frac{u_{\xi\xi}^3}{u_\xi^{3/2}}\right) + \mathcal{O}(b^{13/2}). \tag{2.7}$$

Here we have kept only the terms necessary to get a non-trivial equation. Now, under the long wavelength approximation, we can neglect the terms of order $\mathcal{O}(b^{13/2})$. Setting the bookkeeping parameter b back to 1, we get

$$u_{\xi\xi} = \frac{3}{2}\sqrt{u_\xi}u_{\xi\xi} + \frac{1}{8}\left(\sqrt{u_\xi}u_{\xi\xi\xi\xi} + \frac{u_{\xi\xi}u_{\xi\xi\xi}}{\sqrt{u_\xi}} - \frac{1}{8}\frac{u_{\xi\xi}^3}{u_\xi^{3/2}}\right). \tag{2.8}$$

This equation was solved by Nesterenko [33]. A localised solution is

$$v(\xi) = \frac{\mathrm{d}u}{\mathrm{d}\xi}(\xi) = \begin{cases} \frac{25}{16}\cos^4\left(\frac{2\xi}{\sqrt{10}}\right) & \text{if } |\xi| < \sqrt{10}\pi/4, \\ 0 & \text{if } |\xi| > \sqrt{10}\pi/4. \end{cases} \tag{2.9}$$

This solution qualitatively matches our numerical simulations of the solitary wave in Figure 2.3. Our numerical solution is not a perfect solitary wave, because it leaks energy to the left. However, the travelling wave profile still qualitatively looks like the solution predicted by Nesterenko. This comparison was performed in greater details by Chatterjee [6]. He found that the solution of Nesterenko had the right qualitative shape but was not correct quantitatively. He devised better approximations by considering the nonlinear system as a perturbation of the linear one, *i.e.* setting the contact force as $F = A\delta^{2+\varepsilon}$ and expanding the solution in powers of ε. The solution of Nesterenko has also been tested experimentally [8], once again with a good qualitative agreement.

2.5 The Diatomic Chain

We will later see that some of the more interesting phenomena in Hertzian lattices are not available on an homogeneous lattice of the form described above. Therefore, we will consider a simple generalisation, a diatomic chain formed with two different types of grains (for

instance, alternating spheres of aluminium and stainless steel), differing by their masses and material properties (Young's modulus and Poisson's ratio).

This model was introduced in recent experiments [36]. Those experiments use interspersed sensors to probe the dynamics of the chain. These sensors record the forces exerted on a few beads. The spectral content of these forces allows for the experimental detection of breathers. We will mainly use displacements in our analytical and numerical study for easiness of use, but the results are applicable to the force variables. The setup is represented Figure 2.4.

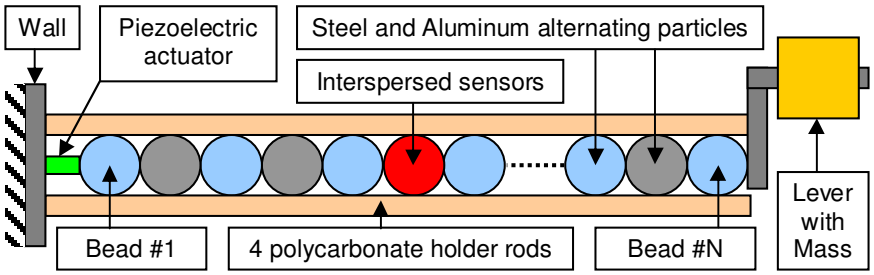

Figure 2.4: Experimental setup used to probe the behaviour of the diatomic granular chain. From [3] with permission.

To model this setup, one must use the full version of Hertz's law describing the contact two different spheres. For two spheres of type 1 and 2, this is [3]

$$A = \left[\frac{3}{4}\sqrt{\frac{1}{R_1}+\frac{1}{R_2}}\left(\frac{1-\nu_1^2}{E_1}+\frac{1-\nu_2^2}{E_2}\right)\right]^{-1}$$

with the same notation as before. The governing equation is now

$$m_n\ddot{u}_n = A\left[\Delta-(u_n-u_{n-1})\right]_+^{3/2} - A\left[\Delta-(u_{n+1}-u_n)\right]_+^{3/2} \tag{2.10}$$

and the linearised equation is

$$m_n\ddot{e}_n = K(e_{n+1}-2e_n+e_{n-1}), \tag{2.11}$$

with the same K as before.

These equations are the same as before, except that the mass is now allowed to change between sites: $m_n = m_1$ when site number n corresponds to a sphere of type 1, $m_n = m_2$ when the sphere is of type 2. The numerical values we use are given in Table 2.1.

Name	Symbol	Value for type 1	Value for type 2
Radius	R	9.525 mm	9.525 mm
Mass	m	9.75 g	28.84 g
Young's modulus	E	73.5 GPa	193 Gpa
Poisson's ratio	ν	0.33	0.3
Stiffness constant	A	$5.46\ \mathrm{N}\,\mu\mathrm{m}^{-3/2}$	
Compression force	F_0	20 N	
Compression at equilibrium	Δ	$2.38\,\mu$m	
Characteristic time	$\sqrt{\frac{m_1\sqrt{\Delta}}{A}}$	$0.05\,\mu$s	
Number of sites	N	81	

Table 2.1: Numerical values used in experimental studies [3]. We use these values in numerical simulations.

Let us examine what the effect of this new model is on the linear spectrum, that is, the plane waves solutions of (2.11). This time, we cannot use the simple ansatz $e_n = e^{i(\omega t - qn)}$, because the two types of beads change the profile of linear waves. To avoid that problem and put our equations in the framework we used to guess the ansatz, we may formally rewrite the linearised equations in the two-dimensional variables $\mathbf{X}_n = (e_{2n}, e_{2n+1})$ and obtain a spatially homogeneous system, to which we can apply our ansatz $\mathbf{X}_n = \mathbf{X}e^{i(\omega t - qn)}$. Going back to our system, this leads to $e_n = E_n e^{i(\omega t - qn)}$, with $E_n = \mathbf{X}^1 = x$ if n is even, $E_n = \mathbf{X}^2 = y$ if odd.

Plugging this ansatz into the linearised system, we get the two equations

$$\begin{cases} -A\omega^2 = K/m_1(-2x + 2y\cos q), \\ -B\omega^2 = K/m_2(-2x + 2y\cos q). \end{cases}$$

This is a linear system in x and y, in the matrix form

$$M \begin{pmatrix} x \\ y \end{pmatrix} = 0,$$

with

$$M = \begin{pmatrix} \omega^2 - 2K/m_1 & 2K/m_1 \cos q \\ 2K/m_2 \cos q & \omega^2 - 2K/m_2 \end{pmatrix}.$$

This has a solution with nonzero x and y if and only if M is singular. Using the condition $\det M = 0$ yields the equation

$$\begin{aligned} (\omega^2 - 2K/m_1)(\omega^2 - 2K/m_2) - \frac{4K^2}{m_1 m_2}\cos^2 q = 0 \\ \implies \omega^4 - 2K(1/m_1 + 1/m_2)\omega^2 + \frac{4K^2}{m_1 m_2}\cos^2 q = 0. \end{aligned}$$

This is a quadratic in ω^2, which we can solve to get

$$\begin{aligned}\omega^2 &= K\left[1/m_1 + 1/m_2 \pm \sqrt{(1/m_1 + 1/m_2)^2 - \frac{4}{m_1 m_2}\sin^2 q}\right] \\ &= K\left[1/m_1 + 1/m_2 \pm \sqrt{1/m_1^2 + 1/m_2^2 + \frac{2}{m_1 m_2}\cos(2q)}\right]. \end{aligned} \tag{2.12}$$

This is the dispersion relation of the diatomic chain, generalising (2.4) to the diatomic case. Indeed, (2.4) is found by trigonometric identities as a special case when $m_1 = m_2$.

The first thing to note in this equation is that the $\pm$ sign defines two separate regions for ω, which are called *acoustic* (for $-$ sign) and *optical* (for $+$ sign) frequency bands, in reference to similar concepts in solid state physics [24]. The acoustic band runs from $\omega^2 = 0$ to $\omega^2 = 2K/m_2$ (assuming $m_2 > m_1$, as in Table 2.1), while the optical band runs from $\omega^2 = 2K/m_1$ to $\omega^2 = 2K(1/m_1 + 1/m_2)$. Therefore, the band structure of our system is characterised by a frequency gap between the acoustic and optical bands. It is in this gap that breathers have been found.

The main difference between acoustic and optical band can be found by looking at the signs of the elements of M. For $q \in [-\pi/2, \pi/2]$, the signs are

$$M = \begin{pmatrix} - & + \\ + & - \end{pmatrix} \text{ in the acoustic band,}$$
$$M = \begin{pmatrix} + & + \\ + & + \end{pmatrix} \text{ in the optical band.}$$

Because $M\begin{pmatrix} x \\ y \end{pmatrix} = 0$, we see that x and y have the same sign in the acoustic band, and opposite signs in the optical band: heavy and light beads move in phase in the acoustic band, and in antiphase in the optical band.

The results are summarised in Table 2.2, which indicates the frequency range of both bands.

Name	q	ω^2	f (kHz)
Lower acoustic	0	0	0
Upper acoustic	$\pm\pi/2$	$2K/m_2$	4.71
Lower optical	$\pm\pi/2$	$2K/m_1$	8.10
Upper optical	0	$2K(1/m_1 + 1/m_2)$	9.37

Table 2.2: Band structure for the diatomic chain, and numerical values with the data of Table 2.1.

The band gap between the acoustic and optical band allows nonlinear vibrations in this frequency gap to avoid contact with small-amplitude waves. This gives rise to breathers.

3 Discrete Breathers

3.1 Definition

The main object of our study is the phenomenon known as discrete breathers (DB) or intrinsic localised modes (ILM). They are time-periodic oscillations that are localised in space, *i.e.* whose amplitude decay as $n \to \pm\infty$ [16]. A typical breather in our diatomic Hertzian lattice is represented Figure 3.1.

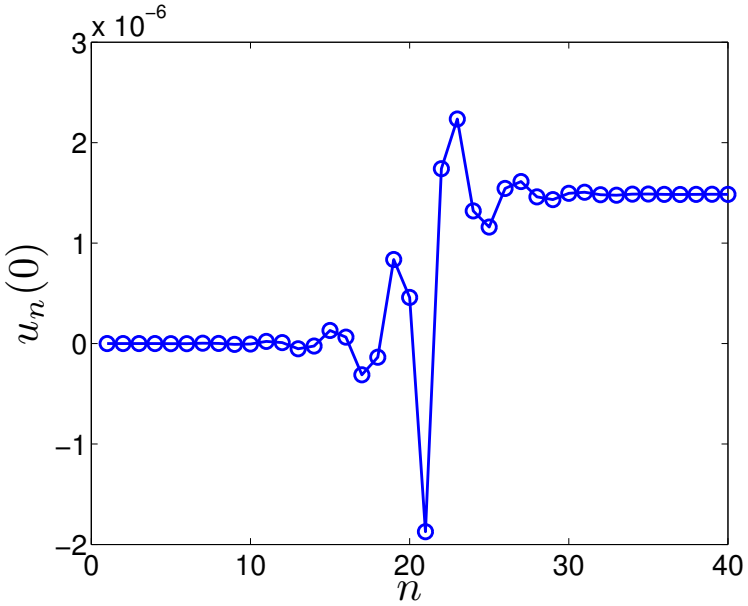

Figure 3.1: Initial conditions in position for a breather with frequency $f = 7.5$ kHz. Initial conditions in velocity are $\dot{u}_n(0) = 0$. This breather was obtained from the numerical methods we develop later on, in Section 3.4.

This breather oscillates by itself, without transmitting any motion to the neighbouring sites. It is localised around about 20 sites and exhibits exponential decay, as seen Figure 3.2.

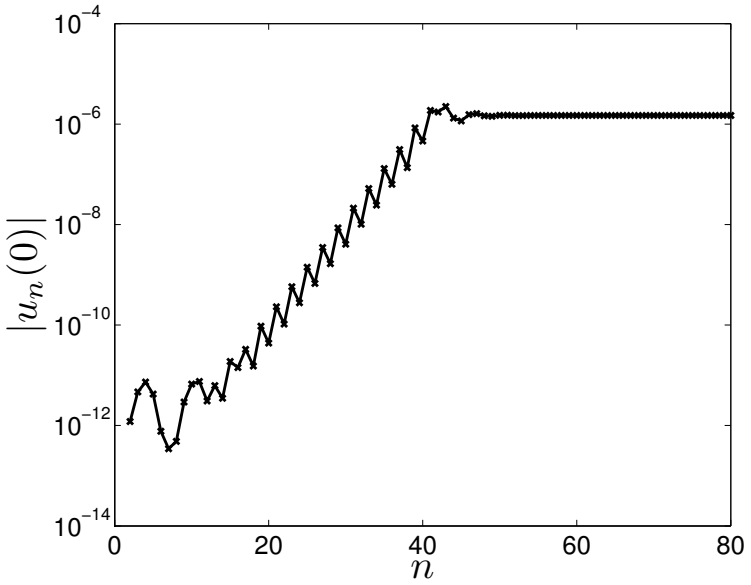

Figure 3.2: Exponential decay of the breather to 0 on the left side. Exponential decay to a constant on the right side can also be shown. The oscillations are due to the heavy/light bead pattern. This numerical computation is seen to be accurate to a relative precision of about 10^{-6}, as chosen in our numerical method.

This localisation is a bit counterintuitive. One might expect that energy would be transmitted to neighbouring sites, creating small waves that would radiate away from the breather. Indeed, our everyday experience tells us that when we pluck a string or make a splash in water, no motion persists without radiating energy away. What is different in our system?

3.2 An Interplay Between Nonlinearity and Discreteness

First, let us assume that such a breather exists: Let $u_n(t)$ be a sequence of functions, satisfying our equations of motion, that is time-periodic with period T_b and spatially localised:

$$\forall t \in \mathbb{R}, \quad u_n(t + T_b) = u_n(t),$$
$$\lim_{n \to \pm\infty} \sup_{t \in \mathbb{R}} |u_n| = c_\pm,$$

where $c_\pm$ represents the constant deformation of the lattice at both ends. We will take $c_- = 0$ for convenience, without loss of generality because of the shift invariance $u_n \to u_n + c$.

Then, we expand $u_n(t)$ in Fourier series:

$$u_n(t) = \sum_{k \in \mathbb{N}} \hat{u}_n^k \, e^{i\Omega_b k t}, \tag{3.1}$$

with $\Omega_b = \frac{2\pi}{T_b}$.

Because the breather is localised, $u_n(t) - u_{n-1}(t)$ is small as $n \to \pm\infty$ and $u_n(t)$ approximately satisfies the linearised equations (2.11). Using the Fourier decomposition (3.1), by

linearity, individual Fourier modes $\hat{u}_n^k\, e^{i\Omega_b k t}$ must also satisfy the linearised equations. This leads to

$$m_n k^2 \Omega_b^2 \hat{u}_n^k = K(2\hat{u}_n^k - \hat{u}_{n+1}^k - \hat{u}_{n-1}^k). \tag{3.2}$$

Physically, this is the equation that determines the amplitudes $\hat{u}_n^k$ for a sinusoidal signal with frequency $k\Omega_b$. When $k\Omega_b$ belongs to the linear spectrum, then $\hat{u}_n^k$ represents an extended plane wave. However if $\hat{u}_n^k$ is extended for some k, then u_n cannot be localised. Hence, the nonresonance condition

$$k\Omega_b \neq \omega_q \tag{3.3}$$

must be satisfied for all q and k. A more rigorous version of this argument, based on Reference [14], is given below.

First, the analysis of (3.2) is cumbersome because m_n depends on n. Thus we restrict ourselves to the case where $m_n = m$ is uniform, and just mention that the result (the nonresonance condition) is the same for our diatomic chain.

Mathematically, (3.2) is a linear two-stage recurrence relation, of the form $\hat{u}_{n+1}^k = a\hat{u}_n^k + b\hat{u}_{n-1}^k$. It is solved by using the ansatz $\hat{u}_n^k = \rho^n$ and solving for ρ. The result of the calculation is that if $k\Omega_b = \omega_q = 2\sqrt{\frac{K}{m}}\sin(q/2)$ for some q, then the solution is

$$\hat{u}_n^k = \alpha e^{iqn} + \beta e^{-iqn}. \tag{3.4}$$

If, on the contrary, $k\Omega_b \neq \omega_q$ for all q, then the general solution is

$$\hat{u}_n^k = \alpha\rho^n + \beta\rho^{-n} \tag{3.5}$$

with $|\rho| > 1$.

Only the second form (3.5) is compatible with a localised solution, by choosing $\alpha = 0$ when $n > 0$, and $\beta = 0$ when $n < 0$. These two choices are compatible, because our analysis is only valid far enough from the breather, and the decomposition $\hat{u}_n^k = \alpha\rho^n + \beta\rho^{-n}$ is not valid for both sides at once. Because only the second form (3.5) is possible, we must have the nonresonance condition $k\Omega_b \neq \omega_q$ for all k and q.

This condition can be interpreted as requiring that none of the harmonics of the breather resonate with small-amplitude waves: there must be a frequency mismatch to prevent energy transfer from the breather to a background of linear waves. Notice that this feature is specific to discrete systems: a continuous system (for instance, the wave equation) generally has an infinite bandwidth, and resonances are unavoidable. We can now understand why it is said that breathers are the result of a constructive interplay between discreteness and nonlinearity [16]: localised oscillations need nonlinearity to have a frequency different from the linear waves, and discreteness to limit the linear bandwidth and avoid resonances.

3.3 Existence

The non-resonance criterion is only a necessary one, and does not by itself guarantee the existence of breathers. Various proofs of existence have been developed in different contexts, starting with the proof by MacKay and Aubry about breathers in Klein-Gordon lattices [26] (a related model, with an extra on-site force), proceeding from the limit of zero coupling (the "anti-continuous limit"). However, most of these proofs are not directly applicable to our system.

One of the mechanisms of localisation consists in a bifurcation from a band edge mode. In a process known as "modulational instability," a plane wave of a frequency corresponding to a band edge bifurcates into a localised mode [16]. A weakly nonlinear analysis can derive analytical approximations of this localised mode, and therefore shows the existence of discrete breathers in the limit where the frequency is close to the band edge. This is a good starting point for existence of breathers in our chain.

The analytical study of plane-wave bifurcations from a band edge in similar lattices was performed by Huang and Hu [22]. The authors considered the $K_2 - K_3 - K_4$ model, where the interacting potential is expanded as a Taylor series, and the three first terms are kept. In our case:

$$\begin{aligned}(\Delta + u_{n-1} - u_n)^{3/2} = \Delta^{3/2} + \frac{3}{2}\Delta^{1/2}(u_{n-1} - u_n) + \frac{3}{8}\Delta^{-1/2}(u_{n-1} - u_n)^2 \\ - \frac{1}{16}\Delta^{-3/2}(u_{n-1} - u_n)^3 + \mathcal{O}((u_{n-1} - u_n)^4),\end{aligned}$$

so that the $K_2 - K_3 - K_4$ model is

$$m_n \ddot{u}_n = \sum_{i=1}^{3} K_i[(u_{i+1} - u_i)^{i-1} - (u_i - u_{i-1})^{i-1}], \text{ where} \tag{3.6}$$
$$K_2 = \frac{3}{2}A\Delta^{1/2}, K_3 = -\frac{3}{8}A\Delta^{-1/2}, K_4 = \frac{1}{16}A\Delta^{-3/2}.$$

This model allows a weakly nonlinear analysis near the band edges. A well-known result [16] is that for a monoatomic chain ($m_n = m$ for all n), a modulational instability takes place: if

$$\frac{K_3^2}{K_2 K_4} < \frac{3}{4},$$

localised modes bifurcate from the upper acoustic band edge. In our case, however,

$$\frac{K_3^2}{K_2 K_4} = \frac{3}{2} > \frac{3}{4},$$

so that this modulational instability does not occur, independently of the values of A and Δ. This means that no breathers are formed via this mechanism in monoatomic lattices.

However, this conclusion does not rule out other types of discrete breathers, such as large-amplitude breathers.

However, on diatomic lattices, the same weakly nonlinear analysis shows that, subject to the condition

$$\frac{K_3^2}{K_2 K_4} > \frac{3}{4},$$

which is satisfied in our model, localised modes bifurcate from the lower optical mode. In this spatially extended mode, heavy beads are stationary, and light beads oscillate in antiphase. This is a plane wave with zero group velocity. In the weakly nonlinear analysis, this mode bifurcates to a stable localised mode, with an amplitude proportional to the square root of the frequency difference between the localised mode and the linear plane-wave mode [22].

Although this $K_2 - K_3 - K_4$ model is just an approximation of the model with the Hertz interaction potential, it supports the existence of breathers in our granular chain and provides an explicit formula in the limit of frequencies close to the lower optical band edge. This approximation will be useful when computing breathers numerically.

3.4 Numerical Computations

3.4.1 Breathers via Newton's method

As the results from the $K_2 - K_3 - K_4$ model are only approximate, we are now interested in obtaining breathers precisely using numerical methods. The first idea is to use direct simulation with specifically chosen boundary conditions. In recent experiments, breathers were found by exciting the lattice with a sine wave of a frequency close to the lower optical cutoff frequency [3]. We can use the same idea numerically, but it then becomes hard to isolate the breather from the background oscillations created by the sine wave. Numerical computations, in contrast to experiments, allow the possibility to use specially crafted initial conditions to form a breather. Reference [18] had some success by using random displacements inside a Gaussian envelope. After an initial phase where the envelope sites radiate energy, one can often observe a breather. Although this does works in some situations, it is an *ad hoc* method with no control on the properties of the resulting breather.

A conceptually cleaner and more precise method is to look for breathers as the solution of an equation: we look for periodic solutions of the equations of motion. To that end, we define by $\mathcal{T}_T$ the Poincaré map

$$\mathcal{T}_T : \{u_n(0), \dot{u}_n(0)\}_{n\in\mathbb{Z}} \to \{u_n(T), \dot{u}_n(T)\}_{n\in\mathbb{Z}}$$

that maps initial conditions in position and velocities to position and velocities at time T. A breather is a fixed point of this map associated with a localised profile.

This operates on an infinite-dimensional space, so we cannot find numerical fixed points of $\mathcal{T}_T$ directly. Rather, we will limit ourselves to a finite number N of sites. Our breathers are exponentially localised, so we can obtain good accuracy by using a limited number of sites. For instance, Figure 3.2 suggests that 80 sites is enough to obtain this particular breather

to a relative accuracy of 10^{-6}. However, breathers of different frequencies might require more sites. In our calculations, we will mostly use $N = 81$, as in the largest experimental studies [3]. Once an appropriate number of sites has been selected, we must choose boundary conditions. As previously mentioned, we use the open boundary conditions $u_0 = u_1$ and $u_{N+1} = u_N$.

With boundary conditions, the map $\mathcal{T}_{T_b}$ is now restricted to a $\mathbb{R}^{2N} \to \mathbb{R}^{2N}$ map, and we can look for fixed points numerically. The simplest possibility is to use a Banach fixed point method, *i.e.* to iterate $\mathcal{T}_{T_b}$ from an initial guess. This amounts to direct simulation of increasing duration. It can work provided our first guess is accurate enough and the map $\mathcal{T}_{T_b}$ is contracting, *i.e.* the breather is linearly stable. However, we will see later that, because of the time-reversal symmetry, our breathers can never be linearly stable in the strict sense. Therefore, such a fixed-point method will not converge in general.

A better choice, that ignores the stability properties, is Newton's method [37]. Newton's method is an algorithm to solve nonlinear systems of equations that proceeds by solving successive linearised problems. Given a map $F : \mathbb{R}^M \to \mathbb{R}^M$, the method to find a solution of $F(x) = 0$ given an initial guess x_0 is to iterate the mapping

$$x_{n+1} = x_n - J_F(x_n)^{-1} F(x_n), \tag{3.7}$$

where $J_F(x_n)$ is the Jacobian (matrix of partial derivatives) of F at point x_n. This method is based on the approximation

$$F(x) = F(x_n) + J_F(x_n)(x - x_n) + \mathcal{O}(||x - x_n||^2). \tag{3.8}$$

Dropping higher order terms (*i.e.* linearising the map around x_n), the equation $F(x) = 0$ is solved by selecting $x = x_n - J_F(x_n)^{-1} F(x_n)$. An illustration of Newton's method in one-dimension is provided in Figure 3.3.

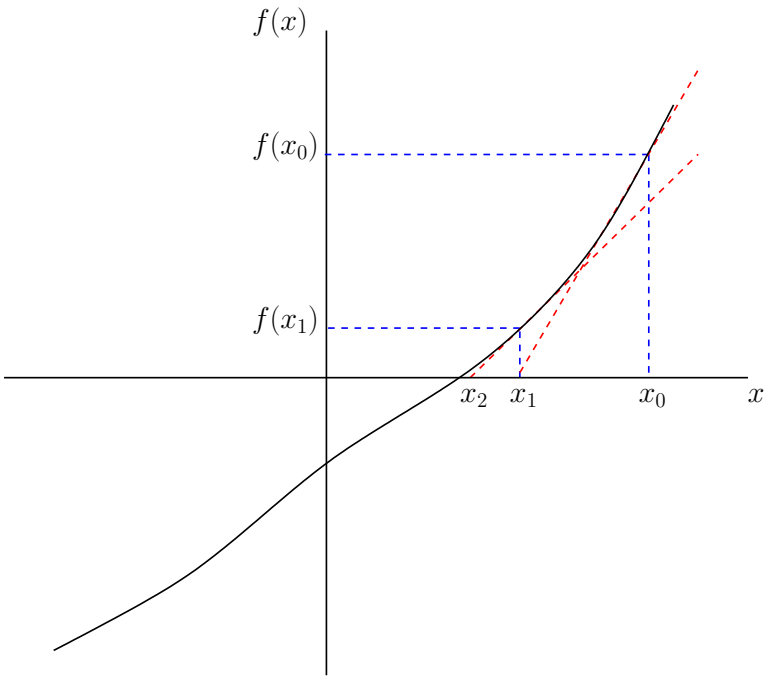

Figure 3.3: Newton's method in one dimension. The function is linearised and the linear problems solved until convergence to a root is achieved.

When no degeneracies are present ($J_F(x)$ is invertible at the root x^*) and the initial guess x_0 is close enough to x^*, this method can be proved to converge quadratically [37].

We use the method introduced by Marín and Aubry [27] and refined by Chen [7]. In particular, we use Newton's method on $F = \mathcal{T}_{T_b} - I$. However, to guarantee convergence of Newton's method, one must take care to remove every degeneracy from the solution. For instance, if $\{u_n(t), \dot{u}_n(t)\}_{1\leq n\leq N}$ is the initial condition for a breather, then so is $\{u_n(t+\tau), \dot{u}_n(t+\tau)\}_{1\leq n\leq N}$ for arbitrary $\tau \in \mathbb{R}$. That is, there is a one-dimensional manifold of solutions to $F(x) = 0$. This causes Newton's method to fail, as it can only be applied to find isolated roots. Numerically, this degeneracy means that $J_F(x)$ is singular, so that the solution to the linear problem (3.8) is not uniquely defined.

This can be solved by only looking for time-reversible breathers, *i.e.* to assume $\dot{u}_n(0) = 0$. This reduces F to a $\mathbb{R}^N \to \mathbb{R}^{2N}$ operator. This time, the dimensions of the two spaces do not match, so we cannot apply Newton's method. Instead, we can use the Newton-Gauss algorithm, an optimisation algorithm that resembles Newton's method, but solves the linearised problem

$$F(x_n) + J_F(x_n)(x - x_n) = 0$$

in the least squares sense, instead of solving it exactly as we do in the $\mathbb{R}^{2N} \to \mathbb{R}^{2N}$ case. This has similar properties to Newton's method, and is numerically found to be very efficient.

3.4.2 Continuation

The algorithm converges quadratically provided the initial guess x_0 is close enough to a root [37]. This means that we have to get an approximate breather by other means to use as initial condition for our iterations. We will use analytical results for this. Usually, breathers are found to be formed by a bifurcation from a simpler state, which provides an appropriate approximation in some limit.

Here, breathers bifurcate from the lower optical mode: this mode is a good approximation to a breather in the limit where the frequency is close to the lower optical frequency. However, the closer we get to this frequency, the more the problem becomes ill-conditioned and the breather becomes spatially extended, requiring a larger number of sites and longer computations. A compromise between those two effects has to be found. Another possibility would be to use the weakly nonlinear approximation from Reference [22], which is even more accurate than the linear optical mode.

Once we have found a breather for a particular frequency close to the optical band, we are interested in finding breathers for lower frequencies. To that end, we will use a *continuation* process. Mathematically, this amounts to finding roots of an equation when a parameter is varied. A justification is provided by the implicit function theorem [25], which is the mathematical basis of the continuation process. This theorem allows us to continue a solution x_0 of an equation for a particular value of a parameter α_0 to other values of the parameter, subject to a non-degeneracy condition. Here we state a finite-dimensional version of the theorem, which admits a generalisation to the case where the solution is to be found in an infinite-dimensional Banach space (this generalisation is used in existence proofs of breathers [26]).

Theorem 1 (Implicit function theorem)**.** *Let $n > 0$ and f be a continuously differentiable function $\mathbb{R}^n \times \mathbb{R} \to \mathbb{R}^n$. If $f(x_0, \alpha_0) = 0$ for some x_0, α_0 and $\frac{\partial f_i}{\partial x_j}(x_0, \alpha_0)$—the Jacobian of f with respect to x, a $n \times n$ matrix—is invertible, then there exists a continuously differentiable function $x = g(\alpha)$ defined on a neighbourhood of α_0, such that $f(g(\alpha), \alpha) = 0$. Furthermore, this function $g(\alpha)$ is the only function having the property $f(g(\alpha), \alpha) = 0$ in this neighbourhood, and it satisfies the differential equation*

$$\frac{\mathrm{d}g}{\mathrm{d}\alpha}(\alpha) = -\left(\frac{\partial f_i}{\partial x_j}(g(\alpha), \alpha)\right)^{-1} \frac{\partial f}{\partial \alpha}(g(\alpha), \alpha). \tag{3.9}$$

In our context, x is the initial conditions for our breather, α the period T_b and f the operator $\mathcal{T}_{T_b} - I$. The theorem then means that, barring any degeneracies, a breather for some period T_b can be continued to a family of breathers $x(T)$ with different periods, yielding a *branch* of solutions. The process can be carried out as long as the Jacobian $\frac{\partial f_i}{\partial x_j}(x_0, \alpha_0)$ is invertible. If this condition fails to hold, then the solution may stop to exist or become non-unique: this generally signals a bifurcation. Notice that the condition is the same as the non-degeneracy condition in Newton's method, suggesting a link between the analytical theory of continuation and the numerical process of Newton's method.

Indeed, the implicit function theorem serves as a basis for a numerical process of branch following called *numerical continuation* [1]. The idea is that we have a breather of initial conditions x_n with period T_n, that is, a root of $\mathcal{T}_{T_n}$, and look for a breather of initial conditions x_{n+1} with period T_{n+1}, that is, a root of $\mathcal{T}_{T_{n+1}}$. If T_{n+1} is close to T_n, we can use iterative algorithms to obtain x_{n+1} from x_n. Then, proceeding by small changes in T_n, we can follow a branch of breathers.

Elaborate algorithms can be devised to obtain x_{n+1}, many of which use a predictor-corrector scheme. The predictor-corrector scheme uses two steps: first, predict a value for x_{n+1}, and then correct this value to ensure it is a zero of $\mathcal{T}_{T_{n+1}} - I$. The predictor step could be implemented using a linear approximation based on the implicit equation—for instance, an explicit Euler method on (3.9)—or simply using x_n (this is what I use for simplicity). Then, the corrector step is implemented using the Newton-Gauss algorithm described in Section 3.4.1. If T_{n+1} is close to T_n and no bifurcation occur, x_{n+1} will be close to x_n (by continuity of g in Theorem 1). Therefore, our predicted value will be close to a root, and the Gauss-Newton algorithm will converge quadratically as long as T_{n+1} is close enough to T_n.

I implemented the method in MATLAB. I used the built-in `ode45` routine (an explicit solver using a pair of Runge-Kutta methods of orders 4 and 5 to provide error control) to numerically integrate differential equations. The Jacobian matrix $J_F(x_n)$ is computed using finite differences (see Reference [37] for accuracy considerations, most importantly the choice of the step size, which has to be of the order of the square root of the function precision for maximum accuracy). The Newton-Gauss process uses MATLAB's backslash operator to solve the least squares system by a QR factorisation of the Jacobian matrix.

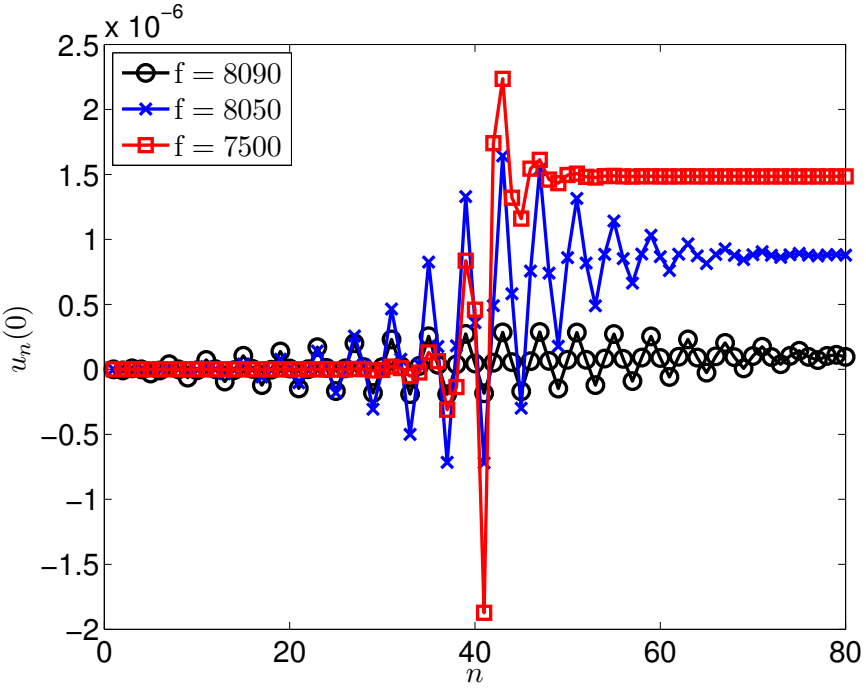

Figure 3.4: Continuation of a breather started near the lower optical band edge at $f \approx 8090$ Hz (circles) down to $f = 7500$ Hz (squares). As seen in Table 2.2, the lower optical frequency is $f = 8094$ Hz. As the frequency decreases, the amplitude increases and the spatial extent decreases.

Figure 3.4 shows a continuation of a breather started close to the lower optical band, in the weakly nonlinear regime, and continued into a strongly nonlinear regime. This was done by small decrements of the frequency f using the continuation process described. Although not shown, the continuation can be performed until one reaches the acoustic band. At this point, an extended oscillatory tail appears and grows as the continuation approaches the upper acoustic frequency. Thus, breathers are numerically found to exist in the whole frequency gap.

The breathers plotted in Figure 3.4 form only one branch of breathers. Reference [39] found another branch of breathers, but they are unstable: we will not focus on them in our study.

3.5 Stability

An important aspect of the dynamics of breathers is their stability. If a breather is too unstable, it is unlikely to be observed in experiments and play an important role in the dynamics of the chain. On the contrary, if it is stable or weakly unstable, it can oscillate for extended periods of time and be experimentally relevant. Therefore, we address the question of the stability of the breathers we found in the previous section.

The simplest way to test their stability is to add small-amplitude noise to the breather

and run a simulation. We find is that the breather is preserved for extended periods of time (tens of periods), even with a small noisy background. That is, even though the extended tail of the breather is perturbed, the core breather oscillations carry on. This effect is seen in Figure 3.5. Therefore, we conjecture that the breather is linearly stable. However, the breather is of course not stable to large perturbations on long timescales.

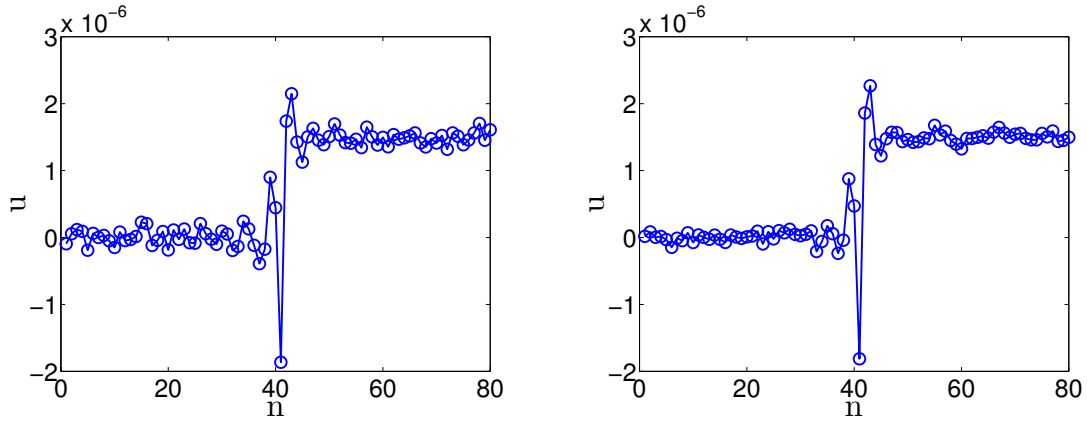

(a) Initial condition.

(b) Final state after 10 periods.

Figure 3.5: Random Gaussian noise of amplitude 10^{-7} on a breather of frequency $f = 7500$ Hz, demonstrating its stability.

To better understand this stability, we linearise the flow of Equation (2.10) around a breather solution $u_n(t)$, and examine the evolution of small perturbations e_n, given by

$$m_n \ddot{e}_n = \frac{3}{2} A \sqrt{\Delta + u_n - u_{n+1}}(e_{n+1} - e_n) - \frac{3}{2} A \sqrt{\Delta + u_{n-1} - u_n}(e_n - e_{n-1}). \tag{3.10}$$

This is a linear equation with time-periodic coefficients. To describe the evolution of these perturbations, it is instructive to study the Poincaré map

$$\mathcal{M} : \{e_n(0), \dot{e}_n(0)\}_{n\in\mathbb{Z}} \to \{e_n(T_b), \dot{e}_n(T_b)\}_{n\in\mathbb{Z}},$$

where T_b is the breather period. This is the analogue of the previously defined $\mathcal{T}_{T_b}$ operator for the linear system (3.10). Information on the behaviour of iterates of this linear map will inform us on the stability of the periodic orbit $u_n(t)$. The associated matrix, called the *Floquet* matrix, is a $2N$-dimensional matrix, which can be studied using its eigenvalues [16].

First, let us note two symmetries. First, because the system is real, if λ is an eigenvalue of $\mathcal{M}$, then so is λ^*. Second, the system is time-reversible: if λ is an eigenvalue, then so is $1/\lambda$, because if $e_n(t)$ is such that $e_n(T_b) = \lambda e_n(0)$, then we can reverse the velocities and run the equation backwards to obtain another sequence of functions f_n such that $f_n(T_b) = e_n(0) = \frac{1}{\lambda} e_n(T_b) = \frac{1}{\lambda} f_n(0)$. This constrains the possible behaviour of eigenvalues and allows for a detailed investigation of their behaviour, using Floquet theory.

Although this theory is hard to apply to our particular case, it is a simple matter to obtain the eigenvalues numerically. Indeed, one can integrate the linearised equations (3.10) for initial conditions where all components except one are zero. This builds the Floquet matrix M, and standard algorithms (such as MATLAB's `eig` function) can then be applied to obtain the eigenvalues.

Once this matrix is computed and its eigenvalues obtained, we can explain the behaviour of $\mathcal{M}$ by analysing the eigenvalues, also known as Floquet multipliers. If a multiplier has modulus larger than 1, then exciting the lattice with the corresponding eigenmode will have perturbations growing by a factor of $|\lambda| > 1$ every period, in the linear regime. Conversely, perturbations associated with a multiplier with modulus smaller than 1 will decay. We now see that the breather cannot be linearly stable in the usual strict sense, meaning that all its Floquet multipliers have modulus strictly smaller than 1, for if $|\lambda| < 1$, then $\frac{1}{\lambda}$ is also an eigenvalue, with $|\frac{1}{\lambda}| > 1$. This comes from the time reversibility of the equations. The only hope for breather stability is that all the multipliers lie on the unit circle. Even then, the breather might be unstable, and its linearisation grow polynomially in case of repeated eigenvalues. The only guarantee that this criterion gives us is that no perturbation will grow exponentially in the linear regime. We call breathers satisfying this criterion *marginally stable* breathers.

The analysis is complicated by finite-size effects [28], causing weak instabilities (multipliers only off from the unit circle by a small amount) that disappear in the limit of an infinite system. Instabilities in the infinite chain are caused by multipliers of modulus significantly greater than 1, associated with localised eigenmodes (which are not sensitive to size effects, in contrast to extended eigenmodes).

The matrix M is related to the Newton's method that we used to obtain breathers. Indeed, the Jacobian of the nonlinear operator $\mathcal{T}_{T_b}$ is exactly our matrix M, for both describe what happens to an infinitesimally small perturbation of the breather after one period. This provides an alternative way of computing the Jacobian in Newton's method, and integrating (3.10) is often more accurate than using finite differences. It also allows for an inexpensive stability check, because we do not need to recompute the matrix M, but we can reuse the one from Newton's method.

We perform this study on the breathers found by numerical continuation in Section 3.4. Excluding finite-size instabilities, the breathers we are interested in (*i.e.* the stable branch, not the unstable branch found in Reference [39]) are generally marginally stable, except for a small band of frequencies between about 7900 to 8000 Hz, just below the lower optical band. In this band, a pair of eigenvalues leaves the unit circle, causing a strong instability (reaching $|\lambda = 1.5|$). Because a change of stability is generally linked to a bifurcation, this result is consistent with a bifurcation into two branches of breathers (one stable and one unstable) just below the lower optical frequency, as found in Reference [39], which analysed the same system in a different parameter regime. Figure 3.6 demonstrates the method on both marginally stable and unstable breathers.

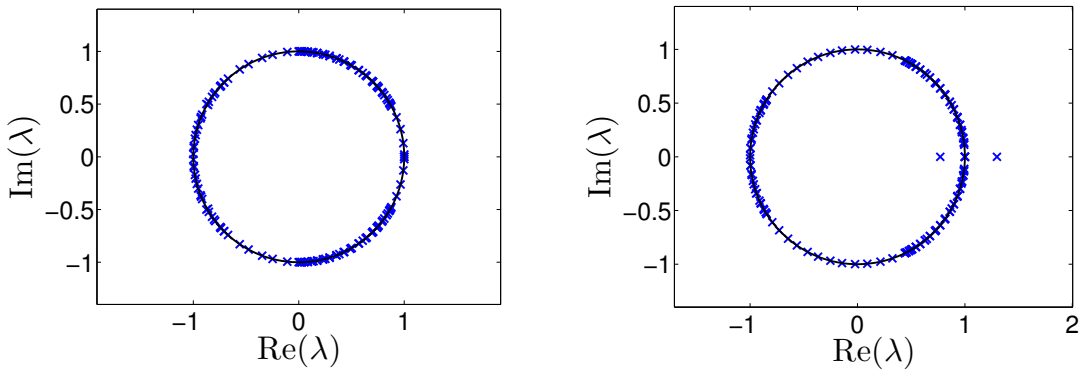

(a) Eigenvalues of a breather of frequency $f = 7500$ Hz.

(b) Eigenvalues of a breather of frequency $f = 7950$ Hz.

Figure 3.6: Multipliers of both (a) marginally stable and (b) unstable breathers.

4 Fano Resonances

4.1 Definition

One of our goals in this project is to understand whether or not *Fano resonances* can occur in the granular chain. Fano resonances were first introduced in spectroscopy, when studying the absorption spectrum of light by atoms. For instance, projecting white light through Argon gas and examining at the frequency content of the transmitted light reveals absorption of a series of frequencies, which are directly linked to the microscopic properties of Argon atoms [29]. A more complex effect was observed by Beutler [2], who noticed unusually sharp asymmetric profiles in those spectra. In particular, a remarkable feature was a point of zero transmission. A theoretical explanation was then proposed by Fano [12]. The simplicity and applicability of this analysis made it a standard tool in many fields of physics [29].

Central to Fano's analysis is the concept of interaction between two propagation path, and destructive interference leading to zero transmission of an incoming wave (perfect reflection). In the case of the absorption of light by atoms, two effects interfere with each other. First, the well-known ionisation process, whereby an electron is detached from an atom by incident radiation. Second, a more subtle process known as autoionisation, including the Auger effect, where an inner shell electron is removed, and an electron from a higher energy level relaxes into this vacant lower energy level, imparting the transition energy to an outer shell electron, which escapes from the atom to create an ion. The quantum superposition of these two effects generates interferences that lead to resonant suppression of transmission. This is the Fano effect.

Fano's analysis led to the formula [29]

$$\sigma(\alpha) = \frac{(\alpha + \beta)^2}{\alpha^2 + 1}, \tag{4.1}$$

where σ is the (unnormalised) transmission coefficient, $\alpha = \frac{\omega - \omega_0}{\Delta\omega}$ is a normalised parameter

representing the deviation from the resonance frequency ω_0, and β is an empirical shape parameter.

This profile possesses a minimum at $\sigma = 0$ for $\alpha = -\beta$, and a maximum at $\sigma = 1 + \beta^2$ for $\alpha = 1/\beta$. Three representative regimes—for $\beta = 0$, $\beta = 1$, and $\beta \to \infty$— are plotted in Figure 4.1.

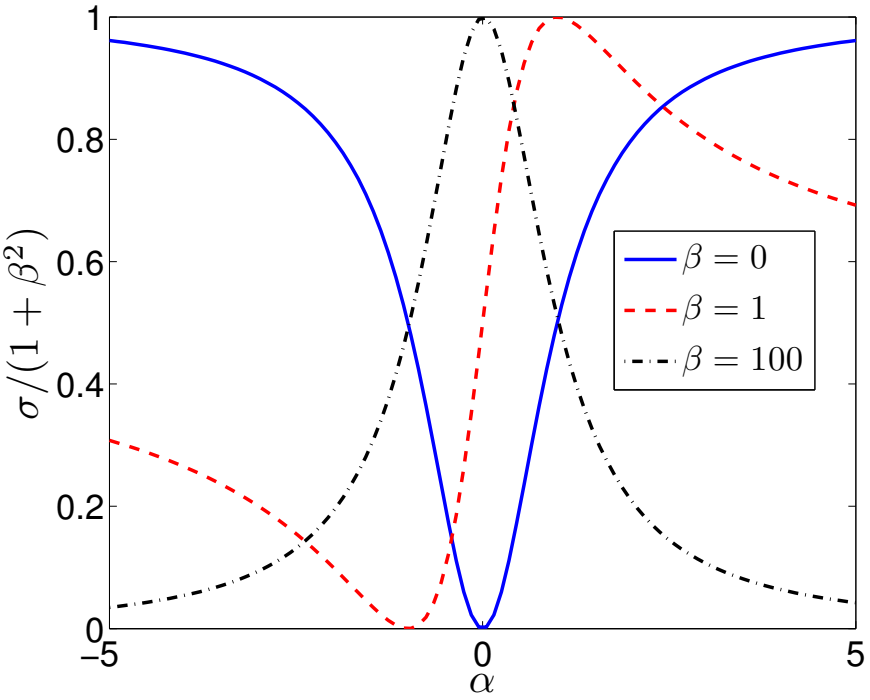

Figure 4.1: Equation (4.1) for different values of the parameter β.

When β is large, we observe the usual resonance phenomenon, where a system displays large amplitudes at its resonance frequency. However when β decreases, a point of zero transmission appears at $\alpha = -\beta$, leading to a characteristic asymmetric shape, with a sharp transition from resonance to anti-resonance. When β goes to zero, the resonance moves to infinity and we only observe a symmetric anti-resonance.

We will now consider progressively more complicated examples of Fano resonances, culminating in Fano resonances in the scattering of plane waves by discrete breathers in waveguide arrays, before examining the possibility of Fano resonances in the granular chain.

4.2 A Simple Example: Coupled Oscillators

4.2.1 Resonances

First, let us recall the phenomenon of resonance in a simple driven oscillator. Consider a mass-spring system that is excited by a driving force. The displacement x satisfies the

equation

$$\ddot{x} + \omega_0^2 x = F(t).$$

Here ω_0 is the angular frequency of the unexcited system, and $F(t)$ is an external driving force. Consider the case where $F(t)$ is sinusoidal, *i.e.*

$$F(t) = F_0 e^{i\Omega t}.$$

The solution of this system is written

$$x(t) = Xe^{i\Omega t} + Ae^{i\omega_0 t},$$

where A is a free oscillation amplitude dependent on initial conditions, and X is a driven oscillation amplitude chosen so that $Xe^{i\Omega t}$ is a particular solution to the equation of motion. The amplitude of the driven oscillations $Xe^{i\Omega t}$ will depend on Ω: this is a resonance. Inserting

$$x(t) = Xe^{i\Omega t},$$

into the equation of motion yields

$$X = \frac{F_0}{\omega_0^2 - \Omega^2}.$$

Thus, the amplitude of the free oscillations increases as the driving frequency Ω gets close to the natural frequency ω_0. The physical interpretation is that if Ω is close to ω_0, the frequencies agree and the driving force helps the movement, whereas if Ω and ω_0 do not match, the driving force is an obstacle to the movement. At $\Omega = \omega_0$, X becomes infinite. This unphysical result is due to the absence of friction in our model, and can be readily addressed by incorporating a linear dissipative term $\alpha\dot{x}$ in the equations of motion, yielding a finite response when $\Omega = \omega_0$. When dissipation is present, the free oscillations decay as $t \to \infty$, so that after a transient the system undergoes forced oscillations $Xe^{i\Omega t}$.

4.2.2 Fano resonances

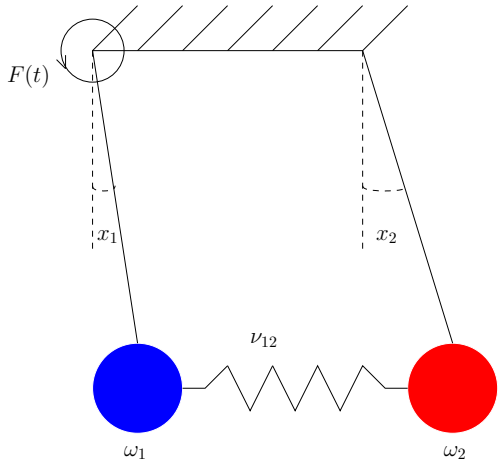

Figure 4.2: Visual representation of the two coupled oscillators setup. This is a schematic representation and does not represent the equation in the text, but gives an intuitive idea of the effects involved in the coupled two-oscillators model. Idea of the figure from Reference [29].

To understand how the superposition of two transmission paths can lead to Fano resonances, following [40], we will use a model consisting of two coupled oscillators, one of which is externally driven. This model, represented schematically in Figure 4.2, is written

$$\begin{cases} \ddot{x}_1 + \omega_1^2 x_1 + \nu_{12} x_2 = F_0 e^{i\Omega t}, \\ \ddot{x}_2 + \omega_2^2 x_2 + \nu_{12} x_1 = 0. \end{cases} \tag{4.2}$$

First, let us consider the case in which $F_0 = 0$. The solutions of the system are obtained by standard methods, and are given by

$$\begin{pmatrix} x_1(t) \\ x_2(t) \end{pmatrix} = \begin{pmatrix} A_1 \\ B_1 \end{pmatrix} e^{i\tilde{\omega}_1 t} + \begin{pmatrix} A_2 \\ B_2 \end{pmatrix} e^{i\tilde{\omega}_2 t},$$

where $\tilde{\omega}_1$ and $\tilde{\omega}_2$ are eigenfrequencies, satisfying the eigenvalue equation

$$(\omega_1^2 - \tilde{\omega}^2)(\omega_2^2 - \tilde{\omega}^2) = \nu_{12}^2, \tag{4.3}$$

and the A and B coefficients are determined by the initial conditions. For small values of the coupling ν_{12}, $\tilde{\omega}_1$ and $\tilde{\omega}_2$ are slight detunings of the original frequencies ω_1 and ω_2.

Now let us consider a nonzero F_0. We consider the driven oscillations given by

$$x_1(t) = X_1 e^{i\Omega t},$$
$$x_2(t) = X_2 e^{i\Omega t}.$$

Solving the resulting system in X_1 and X_2, we get

$$\begin{pmatrix} X_1 \\ X_2 \end{pmatrix} = \frac{F_0}{(\omega_1^2 - \Omega^2)(\omega_2^2 - \Omega^2) - \nu_{12}^2} \begin{pmatrix} \omega_2^2 - \Omega^2 \\ -\nu_{12} \end{pmatrix}. \tag{4.4}$$

There are two things to note. First, the denominator becomes infinite at $\Omega = \tilde{\omega}_1$ or $\Omega = \tilde{\omega}_2$. This is the usual process of resonance, analogous to the one-oscillator case, whereby a system excited at one of its natural oscillation frequencies displays large-amplitude oscillations. Second, $X_1 = 0$ when $\Omega = \omega_2$. In this case, the first oscillator merely acts as a buffer between the driving force and the second oscillator: the resonance with the second oscillator inhibits any motion of the first one. The interaction of these two effects at very close frequencies ω_2 and $\tilde{\omega}_2$ gives rise to a very sharp asymmetric shape, as can be seen Figure 4.3.

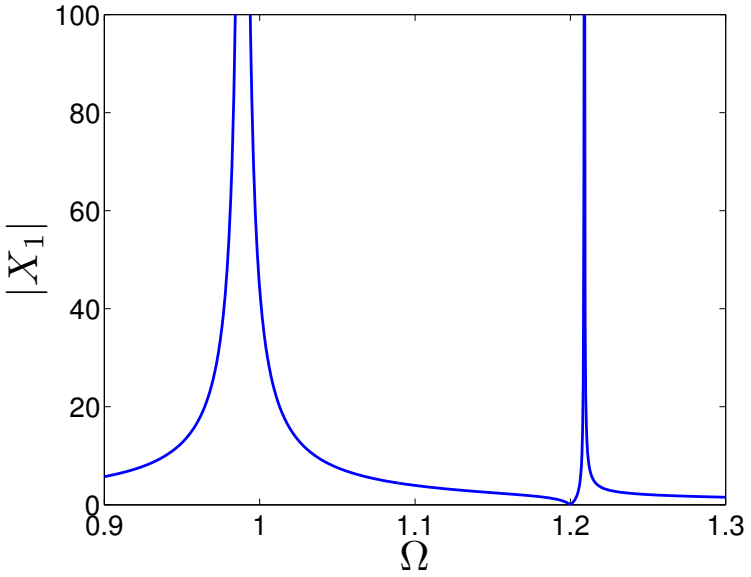

Figure 4.3: Fano resonance for a coupled system of oscillators described by (4.4). The parameters are $\omega_1 = 1$, $\omega_2 = 1.2$, and $\nu_{12} = 0.1$. This choice yields $\tilde{\omega}_1 \approx 0.989$ and $\tilde{\omega}_2 \approx 1.209$. The quantity X_1 is infinite at these frequencies, and zero at $\omega_2 = 1.2$, creating an asymmetric peak near ω_2.

As before, the unphysical result of infinite amplitudes is explained by the lack of friction in (4.2). A model including friction can be found in Reference [40], but the additional complexity does not change the main features of (4.4) and obscures the main point, which is the asymmetric shape produced by the detuning of the eigenfrequencies.

4.3 Fano-Anderson Model

We have seen how an interaction between an anti-resonance and a slightly detuned resonance can lead to very sharp transitions in the transmission spectrum. We will now examine a more

complicated model, the Fano-Anderson model [30]. This is a Hamiltonian lattice like our granular chain, but simple enough that an analytical approach is possible.

This model consists of two subsystems: an infinite system of oscillators ϕ_n with nearest-neighbour coupling C, and an oscillator ψ with frequency Ω. Instead of a second order differential equation like before, and by analogy with quantum mechanics and the Schrödinger equation, we use a complex first order differential equation. Thus, the two systems are

$$i\dot{\phi}_n = C(\phi_{n-1} + \phi_{n+1})$$

and

$$i\dot{\psi} = \Omega\psi.$$

The first system supports plane waves with dispersion relation $\omega_q = 2C\cos q$, and the second system oscillates at frequency Ω. We now link those two systems by including a coupling term V_F between the oscillator number 0 of the chain and the second subsystem:

$$\begin{aligned} i\dot{\phi}_n &= C(\phi_{n-1} + \phi_{n+1}) + V_F\psi\delta_{n0}, \\ i\dot{\psi} &= \Omega\psi + V_F\phi_0. \end{aligned}$$

This is a simplified version of the Fano-Anderson model [29]. We will show that this interaction opens the possibility of a Fano resonance. Indeed, there are now two propagation paths: an incoming wave at $n = 0$ can either pass directly through the chain, or indirectly through the second subsystem. These two propagation paths can interact destructively and cause total reflection.

We look for periodic solutions of these equations:

$$\phi_n(t) = A_n e^{-i\omega t}, \quad \psi(t) = Be^{-i\omega t},$$

where A_n and B are complex amplitudes. This leads to the coupled set of algebraic equations

$$\begin{aligned} \omega A_n &= C(A_{n-1} + A_{n+1}) + V_F B\delta_{n0}, \\ \omega B &= \Omega B + V_F A_0. \end{aligned}$$

Immediately, we obtain

$$B = \frac{V_F A_0}{\omega - \Omega},$$

so

$$\omega A_n = C(A_{n-1} + A_{n+1}) + \frac{V_F^2 A_0}{\omega - \Omega}\delta_{n0}. \tag{4.5}$$

This is a key point to our analysis: for $\omega = \Omega$, the quantity B becomes infinite, which produces an infinite scattering potential at $n = 0$. This infinite potential acts as a barrier and prevents transmission. This is confirmed by the derivation of the transmission coefficient,

which is defined as the square of the ratio of the amplitude of the transmitted wave to the incoming one. We consider the scattering problem given by

$$A_n = \begin{cases} Ie^{iqn} + \rho e^{-iqn}, & n < 0 \\ \tau e^{iqn}, & n > 0 \end{cases}$$

where an incoming wave of amplitude I is separated into a reflected wave of amplitude ρ and a transmitted wave of amplitude τ. Without loss of generality, we will assume that $I = 1$. The transmission coefficient is then given by $T = |\tau|^2$.

Fully solving the problem requires determining the values of three variables: ρ, τ, and A_0. Writing the amplitude equation (4.5) for $|n| \geq 2$ only yields the dispersion relation, which is satisfied by choosing $\omega = \omega_q = 2C \cos q$. Thus, we are left with three equations, (4.5) for sites -1, 0, and 1. This leads to a linear system of three equations for the three unknowns ρ, τ, and A_0. Solving it leads to [30]

$$T = \frac{\alpha_q^2}{\alpha_q^2 + 1}, \tag{4.6}$$

where

$$\alpha_q = \frac{2C \sin q}{V_F^2}(\omega - \Omega) \tag{4.7}$$

is a normalised deviation from the resonance frequency Ω.

The transmission coefficient exactly $T(\omega_q)$ matches the Fano formula (4.1) with shape parameter $\beta = 0$, except for the $\sin q$ dependence of α_q, which is only significant near band edges. Correspondingly, and as conjectured from the scattering potential (4.5), Equation (4.6) includes a point of zero transmission when $\alpha_q = 0$, *i.e.* $\omega = \Omega$. For an incoming wave of that frequency, the second subsystem ψ resonates, and that leads to a resonant suppression of transmission. This effect is the same as in the two-oscillator case, where a resonance on the second oscillator led to a zero amplitude for the first oscillator.

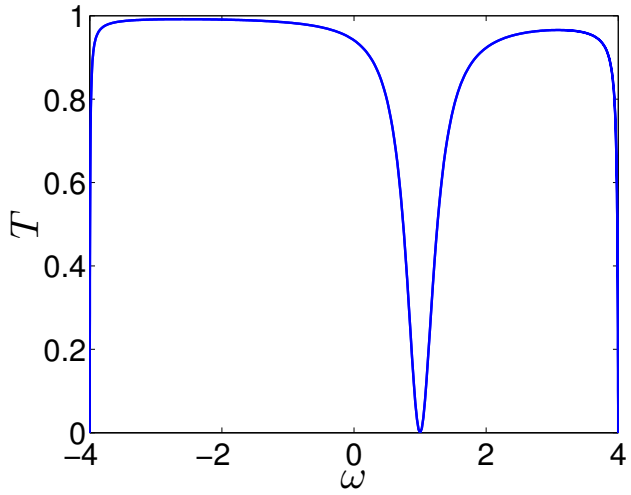

Figure 4.4: Transmission coefficient T as a function of the incoming frequency ω. The anti-resonance is at Ω, and its width scales like V_F^2/C. The parameters for this plot are $C = 2$, $V_F = 1$, and $\Omega = 1$. The zero transmission at endpoints is not linked to the Fano resonance but is instead caused by the vanishing of the group velocity.

This is a particularly simple example. We now study a more complicated model for which an analytical solution is still possible.

4.4 Waveguide Arrays

We consider the model

$$-i\dot{u}_n = u_{n+1} + u_{n-1} + \left(\epsilon - \frac{\beta}{1+|u_n|^2}\right) u_n \delta_{n,n_c}. \tag{4.8}$$

This model was proposed to study the propagation of light in weakly coupled waveguides close to the first band of the band structure [31]. Here u_n is the light amplitude at a guide centred around site n, and the dependent variable is a spatial coordinate. However, we continue to refer to it by t and think about it as a time to maintain consistency with the other models. Ignoring the third term in the right-hand side, it is the first sub-system we studied in the Fano-Anderson model, supporting plane waves with dispersion relation $\omega_q = 2\cos q$. The third term represents an impurity at site n_c. This impurity includes both a linear term, controlled by ϵ, and a nonlinear term, controlled by β. The combination of these two terms allows breathers to form. These are not intrinsic localised modes however, because the localisation is caused by the inhomogeneity of the lattice.

We look for a breather solution with a decaying amplitude and periodic time dependence, centred around the impurity n_c

$$u_n(t) = U_0 x^{|n-n_c|} e^{i\Omega_b t}, \tag{4.9}$$

where Ω_b is the breather frequency, and x is the localisation strength, with $|x| < 1$ (a small x corresponds to a very localised breather).

Inserting this ansatz into our model, and denoting by $g = \frac{\beta}{1+U_0^2}$ the characteristic strength of the nonlinear impurity, we get

$$x = \frac{g-\epsilon}{2} \pm \sqrt{1 + \left(\frac{g-\epsilon}{2}\right)^2},$$
$$\Omega_b = \pm\sqrt{4 + (g-\epsilon)^2}.$$

The plus or minus sign in these equations is chosen so as to impose $|x| < 1$ and depends on the relative values of ϵ and g. If $g > \epsilon$ (large nonlinear impurity), the sign is minus and the breather profile is staggered, with the sites having alternating amplitudes. If $g < \epsilon$ (small nonlinear impurity), the sign is plus and the breather profile is unstaggered.

We now examine the scattering properties of our breather. The linearised equation for small perturbations e_n is

$$-i\dot{e}_n = e_{n+1} + e_{n-1} + \left[\left(\epsilon - \frac{g^2}{\beta}\right) e_n + \frac{g^2}{\beta} U_0^2 e^{2i\Omega_b t} e_n^*\right] \delta_{n,n_c}. \tag{4.10}$$

We consider an incoming wave of frequency $\omega = 2\cos q$. The term $e^{2i\Omega_b t} e_n^*$ in (4.10) will produce a second channel of frequency $2\Omega_b - \omega$. Therefore, we use the two-channels ansatz

$$e_n = a_n e^{i\omega t} + b_n^* e^{i(2\Omega_b - \omega)t}.$$

This leads to the closed coupled set of algebraic equations

$$\omega a_n = a_{n+1} + a_{n-1} + \left[\left(\epsilon - \frac{g^2}{\beta}\right) a_n + \frac{g^2 U_0^2}{\beta} b_n\right] \delta_{n,n_c},$$
$$(2\Omega_b - \omega) b_n = b_{n+1} + b_{n-1} + \left[\left(\epsilon - \frac{g^2}{\beta}\right) b_n + \frac{g^2 U_0^2}{\beta} a_n\right] \delta_{n,n_c}. \tag{4.11}$$

In a Fano resonance, the channel b_n is fully excited and acts as an inhibitor for the propagation of the wave described by a_n. To examine this case, we set $a_{n_c} = 0$ and seek a localised channel of the form $b_n = y^{|n-n_c|}$, with $|y| < 1$. Writing (4.11) for $n = n_c$ and $n \neq n_c$ leads to two algebraic equations coupling ω and y. Solving for ω yields

$$\omega_f = 2\Omega_b \pm \sqrt{4 + \left(\epsilon - \frac{g^2}{\beta}\right)^2}, \tag{4.12}$$

where the plus sign holds if $\epsilon < \frac{g^2}{\beta}$, and the minus sign holds otherwise. Equation (4.12) gives the frequency of the fully excited localised mode b_n. When $\omega = \omega_f$, it is reasonable to expect a Fano resonance, for which the transmission mode a_n is inhibited.

Now we come back to the general case where $a_{n_c} \neq 0$ and compute the transmission coefficient. This is done by considering the scattering problem.

$$a_n = \begin{cases} Ie^{iq(n-n_c)} + \rho e^{-iq(n-n_c)} & \text{when } n < n_c \\ \tau e^{iq(n-n_c)} & \text{when } n \geq n_c \end{cases}$$
$$b_n = b_0 y^{|n-n_c|}.$$

Here, as in the waveguide arrays, I, ρ, and τ are the (complex) amplitudes of the incoming, reflected, and transmitted waves respectively. Without loss of generality, we take $I = 1$, and compute the transmission coefficient $T = |\tau|^2$. Writing the amplitude equations (4.10) for sites $n_c - 1, n_c$ and $n_c + 1$, we obtain three algebraic equations for our three unknowns ρ, τ and b_0. Solving the system for T yields [31]

$$T = \frac{\alpha_q^2}{\alpha_q^2 + 1}, \text{ where} \tag{4.13}$$
$$\alpha_q = \frac{4\sin^2 q}{\Omega_q^2}, \text{ where}$$
$$\Omega_q^2 = \epsilon - \frac{g^2}{\beta} + \frac{g^4 U_0^4}{g^2 - \beta\epsilon \pm \beta\sqrt{|(2\Omega_b - \omega_q)^2 - 4|}}. \tag{4.14}$$

The plus sign holds for $(2\Omega_b - \omega_q) > 2$, and the minus sign holds otherwise.

Equation (4.13) is exactly of the form of the Fano formula (4.1) with shape parameter equal to zero. An anti-resonance occurs when the denominator of (4.14) vanishes, which is when $\omega = \omega_f$, as predicted earlier using the decoupling ansatz $a_{n_c} = 0$.

We now numerically validate these results. Following Reference [31], we use the numerical values $\beta = 10$ and $\epsilon = 5$. We find that ω_f is contained in the linear band when $1 \lesssim U_0 \lesssim 1.9$. We fix $U_0 = 1.4$. We get $\omega_f \approx 0.803$, corresponding to $q \approx 1.57$.

Ideally, we should send a perfect plane wave of wavenumber q_f towards the breather. It is not straightforward to do so however, because we cannot simulate an infinite domain. Therefore, to conduct the numerical experiments, we send incoming waves inside a Gaussian envelope. This forms a localised wavepacket that travels through the chain. However, doing so will extend the frequency content of the wave, which will contain additional frequencies around the plane wave frequency ω_q. Indeed, by the properties of the Fourier transform, if $f(x)$ has transform $\hat{f}(\omega)$, then $f(ax)$ has transform $\frac{1}{|a|}\hat{f}(\frac{\omega}{a})$: localisation in the space domain corresponds to extension in the frequency domain. Therefore, although we need a finite-size wave packet to run simulations, we also need the envelope to be sufficiently extended so that it approximates the frequency content of a plane wave.

More precisely, the initial conditions we use are

$$w_n(0) = e^{iqn} e^{-\frac{(n-n_0)^2}{\sigma^2}} \tag{4.15}$$

where σ controls the width of the envelope (we need $\sigma \gg \frac{1}{q}$ to get a well-defined frequency for the wave packet), and n_0 is the centre of the envelope.

These initial conditions do not define an exact right-travelling wave, but approximate one as $\sigma \to +\infty$. In practise, the wave packet travels to the right without losing its shape as long as σ is large enough.

We integrate the nonlinear equation (4.8) on a chain of size $N = 500$ with a defect at $n_c = 250$. Initial conditions consist of the breather solution (4.9) centred around $n_c = 250$, superposed with a small-amplitude (in our tests, we chose 10^{-2}) wave packet defined by (4.15), centred at $n = 125$ with a width $\sigma = 30$

$$u_n(0) = U_0 x^{|n-n_c|} + 10^{-2} e^{iqn} e^{-\frac{(n-n_0)^2}{\sigma^2}}.$$

The result of the scattering is given Figure 4.5. The wave travels to the right and is reflected by the breather.

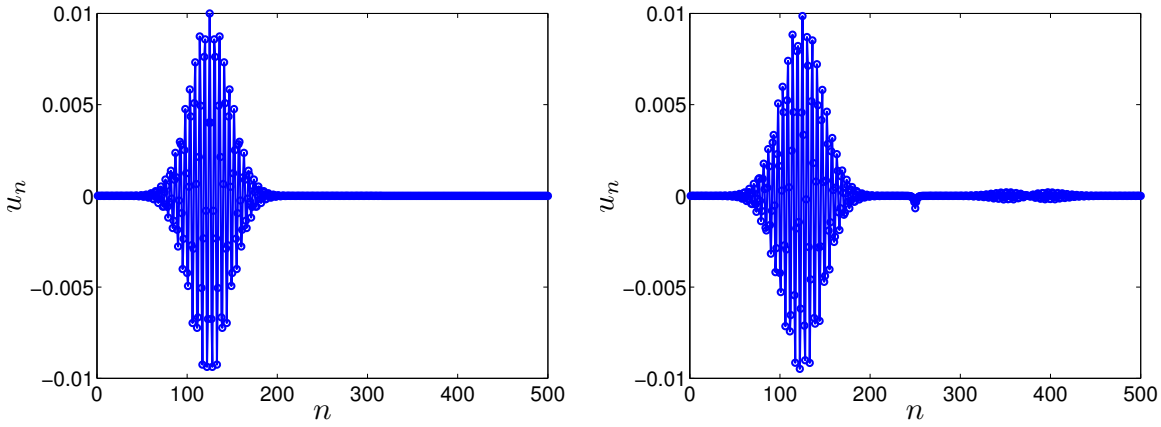

(a) Before the scattering.

(b) After the scattering, when the reflected wave is back to its starting position.

Figure 4.5: Scattering of an incoming wave packet of wavenumber $q \approx 1.57$, corresponding to $\omega = \omega_f$. The wave is nearly perfected reflected, demonstrating a Fano resonance. The breather solution $x^{|n-n_c|}e^{i\Omega_b t}$ has been subtracted from the plots, and we only show the real part of u_n.

On the example of a model for waveguide arrays, following [31], we derived analytically a Fano resonance and validated it numerically. We now turn to the more intricate case of scattering by discrete breathers in FPU chains.

5 Wave Scattering by Discrete Breathers

We have examined the effect of background excitations on breathers when we discussed stability of discrete breathers. We concluded that for stable breathers, small perturbations do not destroy the localised oscillations. On the other hand, breathers will affect those perturbations. To understand this effect, we consider the problem of wave scattering: how

will a breather change the characteristics of incoming waves? By Fourier analysis, this is of relevance not only to plane waves, but also to any infinitesimally small perturbation.

We have seen in Section 4 that the superposition of propagation paths can lead to resonant suppression of transmission, called Fano resonances. We now investigate whether analogous phenomena are possible in granular chains. First, we introduce the theoretical framework that we will use to analyse wave scattering by discrete breathers.

5.1 Theoretical Framework

We start from the linearised equations (3.10) around a breather $u_n(t)$ with period T_b. For a marginally stable breather, all of the Floquet multipliers are located on the unit circle: they are written $\lambda = e^{i\theta}$. This implies that for an eigenvector $e_n(t)$, we have $e_n(t+T_b) = e^{i\theta}e_n(t)$: the evolution of e_n after one period is simply a phase shift. Defining the auxiliary functions $f_n(t) = e^{-i\frac{\theta}{T_b}t}e_n(t)$, we see that these functions are periodic with period T_b. This leads to a Fourier representation of e_n', which in turn implies a representation of e_n in terms of the harmonics

$$e_n(t) = \sum_{k=-\infty}^{\infty} e_n^k e^{i(\frac{\theta}{T_b}+k\Omega_b)t},$$

where $\Omega_b = \frac{2\pi}{T}_b$ is the breather angular frequency and e_n^k is the kth Fourier coefficient.

Now, were the breather not to exist ($u_n(t) = 0$ for all n and t), we know the spectrum θ contains plane waves, which satisfy $\theta = \omega_q T_b$, where ω_q is the frequency of a plane wave of wavenumber q, as described by (2.12). The breather, being exponentially localised, will only slightly modify those plane waves, and $\theta = \omega_q T_b$ will still be a part of the spectrum. Therefore,

$$e_n(t) = \sum_{k=-\infty}^{\infty} e_n^k e^{i(\omega_q+k\Omega_b)t}. \tag{5.1}$$

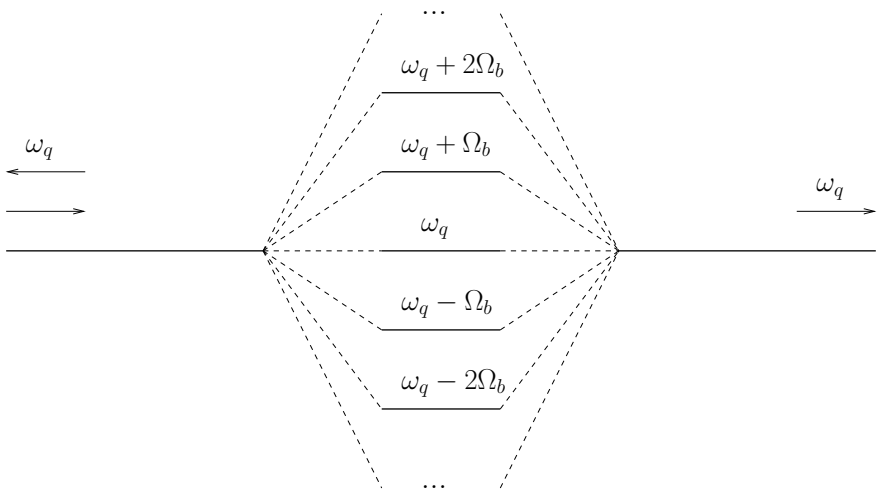

Figure 5.1: Schematic representation of the one-channel scattering process. An incoming wave can excite localised modes, leading to interferences. Idea of the figure from Reference [17].

This is a representation of scattering states as superpositions of plane waves in a discrete ladder of frequencies $\omega_q + k\Omega_b$. It is represented schematically in Figure 5.1. We are interested in the behaviour of the coefficients e_n^k at infinity, because this will determine the transmission properties of incoming waves.

By linearity, the functions $e^{i(\omega_q + k\Omega_b)t} e_n^k$ have to satisfy the linearised equations (3.10). This implies that, for each k, one of two things can happen: either the frequency $\omega_q + k\Omega_b$ belongs to the linear spectrum, or it does not. If it does, then the corresponding vector e_n^k is spatially extended (a plane wave propagates). If it does not, then e_n^k decays exponentially, and the mode is localised. In the first case, we say that the channel k is *open*; in the second, we say that it is *closed*. If more than one mode is open, we are dealing with *multi-channel scattering*, while if only the mode $k = 0$ is open, it is a *single-channel scattering*. In the case of single-channel scattering, a single incoming wave produces a reflected and a transmitted wave of the same frequencies. In the case of former case however, additional transmitted and reflected waves of frequencies $\omega_q + k\Omega_b$ are created.

Due to the limited bandwidth of our chain, only a finite number of channels can be opened by a breather. In fact, for our parameter values (Table 2.1), only the channels -1 or $+1$ can be open in addition to channel 0. For instance, Figure 5.2 represents a scattering situation where the channel $k = +1$ is opened.

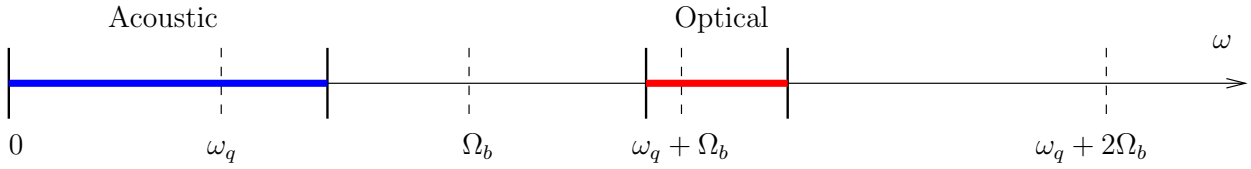

Figure 5.2: A multi-channel scattering situation with channel $+1$ opened. The incoming acoustic wave at frequency ω_q creates an optical wave at frequency $\omega_q + \Omega_b$.

Thus, we can have three cases: a plane wave passing through the breather, an acoustic wave giving rise to a secondary optical transmitted wave, and an optical wave giving rise to a secondary acoustic transmitted wave.

5.2 Multi-Channel Scattering

We now focus on the breather of Figure 3.1 and illustrate the theoretical results with two computational experiments. This is original work. We use an acoustic wave of wavenumber $\pi/10$ and frequency 1270 Hz, and an optical wave of wavenumber $\pi/3$ and frequency 8530 Hz (recall from Table 2.2 that the acoustic band runs from 0 to 4710 Hz and the optical band from 8100 to 9370 Hz). We chose these frequencies to observe a two-channel scattering in both cases. In both cases we used the breather of Figure 3.1 centred at site $n = 500$ with a chain of $N = 1000$ sites. The experiments will serve as a preliminary verification of the validity of the theoretical framework, and as a testbed for the numerical method we will use in Section 5.3 to probe Fano resonances.

As in the numerical simulations that we performed on the waveguide arrays, we use an incoming wave packet localised inside a Gaussian envelope

$$\begin{aligned} w_n(0) &= W_n \cos(-qn) e^{-\frac{(n-n_0)^2}{\sigma^2}}, \\ \dot{w}_n(0) &= -\omega_q W_n \sin(-qn) e^{-\frac{(n-n_0)^2}{\sigma^2}}, \end{aligned}$$

where the coefficients W_n take different values for even and odd sites, and are chosen so that

$$\begin{aligned} e_n(t) &= W_n \cos(\omega_q t - qn), \\ \dot{e}_n(t) &= -\omega_q W_n \sin(\omega_q t - qn) \end{aligned}$$

is an exact plane wave solution to the linear equations (2.11).

We illustrate the scattering of these travelling wave packets by a breather at the centre of the chain in Figure 5.3 for an incoming acoustic wave and in Figure 5.4 for an incoming optical wave. These results were obtained by integration of the linearised equations (3.10) around the breather depicted in Figure 3.1, and we checked that they hold in the weakly nonlinear case of the nonlinear equations, with a perturbation amplitude 10^4 times smaller than the amplitude of the breather. We only represent the perturbations corresponding to the waves, not the breather itself.

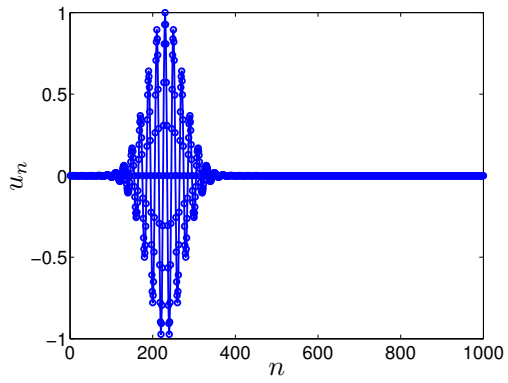

(a) Before the scattering.

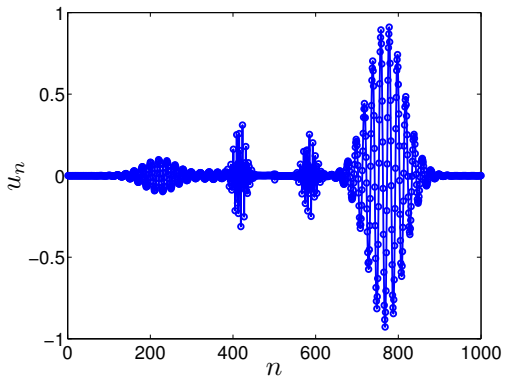

(b) After the scattering of the acoustic wave into an acoustic and an optical wave.

Figure 5.3: Multi-channel scattering of an incoming acoustic wave packet of frequency $f = 1270$ Hz by a breather centred at $n = 500$. The plot on the left represent the incoming wave packet, and the plot on the right represent the state of the chain after the scattering has taken place, when the transmitted wave packet (right) has passed through the breather, and generated a secondary optical wave packet (second from the right) and two reflected wave packets.

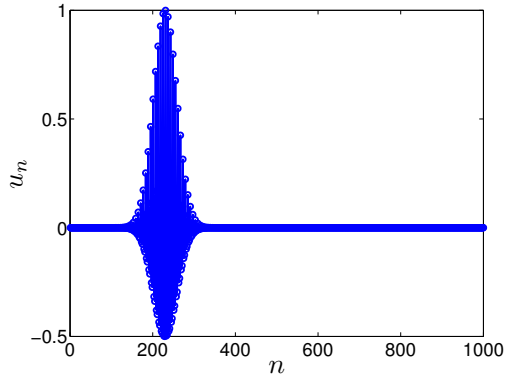

(a) Before the scattering.

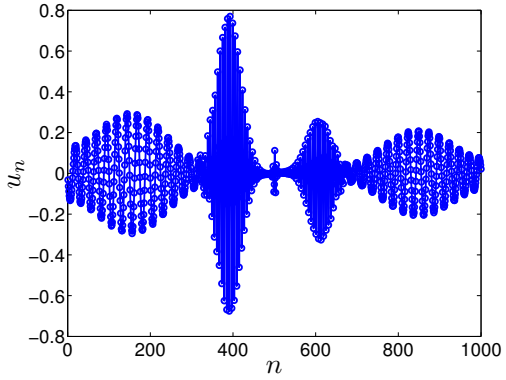

(b) After the scattering of the optical wave into an optical and an acoustic wave.

Figure 5.4: Multi-channel scattering of incoming optical wave packet of frequency $f = 8530$ Hz by a breather centred at $n = 500$.The plot on the left represent the incoming wave packet, and the plot on the right represent the state of the chain after the scattering has taken place, when the transmitted wave packet (second from the right) has passed through the breather and generated a secondary acoustic wave packet (right) and two reflected wave packets.

The observations in these figures are consistent with the theory: the breather opens another channel (channel $+1$ or -1, at frequency $\omega_q \pm \Omega_b$), leading to the emission of an

extra pair of transmitted and reflected wave. As a result, a superposition of an acoustic and an optical wave propagates through the chain. For our parameter values, acoustic waves have a higher group velocity than optical waves, so acoustic wave packets travel faster than optical ones, and we observe a clean separation.

This interpretation can be checked using the discrete Fourier transform (computed using the fast Fourier transform algorithm [37]) in the time domain: wave packets of a particular frequency show up as peaks in the spectral density $|\hat{u}_n(f)|$. This computation is performed in Figure 5.5 for an incoming acoustic wave, and in Figure 5.6 for an incoming optical wave. Far from the breather, only open channels are significant, while inside the breather, closed channels are active as well.

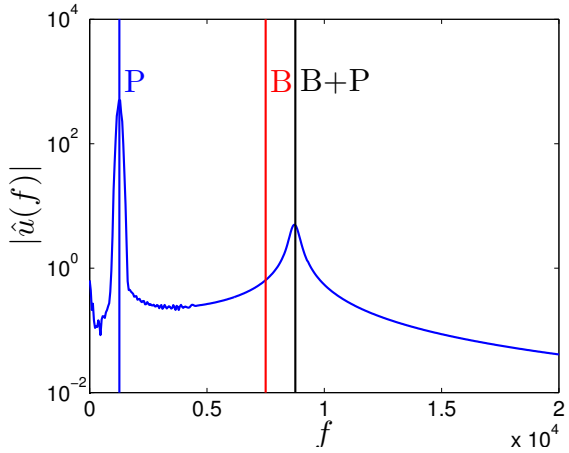

(a) Frequency content at site $n = 400$, far from the breather. Channel number 0 and channel number $+1$, of frequency $\omega_q + \Omega_b$, is open.

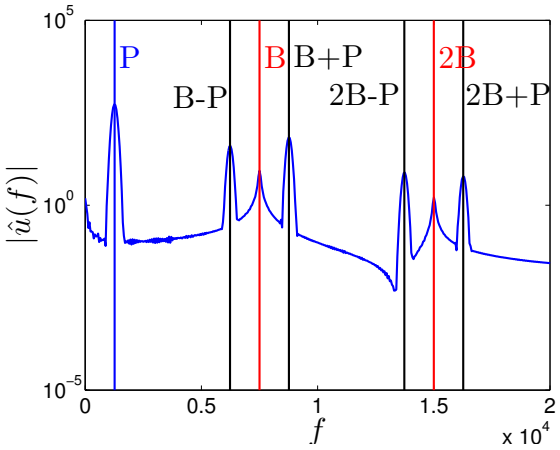

(b) Frequency content at site $n = 500$, in the middle of the breather. In addition to open channels 0 and $+1$ that are seen far from the breather, closed channels -2, -1, and $+2$ are visible.

Figure 5.5: Discrete Fourier transforms of the time evolution far from the breather and in the middle of the breather for the experiment in Figure 5.3 with an incoming acoustic wave. The notations are P for the incoming phonon (linear wave) frequency and B for breather frequency, so that for instance $B + P$ corresponds to channel number 1, with frequency $\omega_q + \Omega_b$.

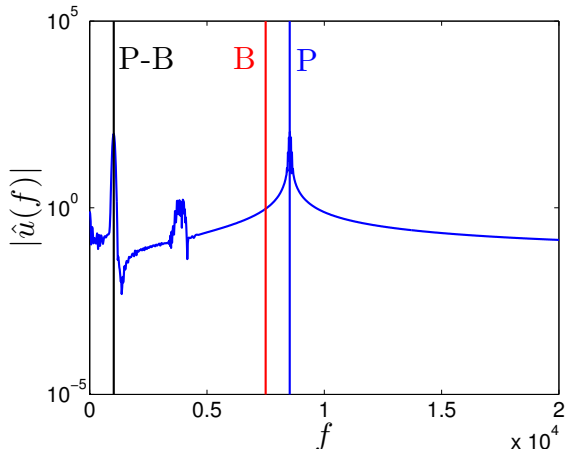

(a) Frequency content at site $n = 400$, far from the breather. Channel number -1, of frequency $\omega_q - \Omega_b$, is open.

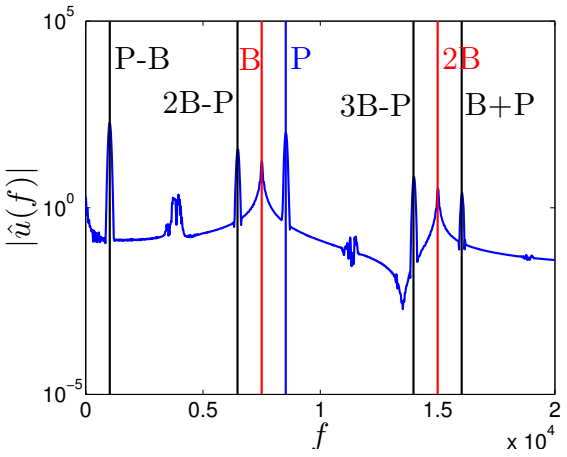

(b) Frequency content at site $n = 500$, in the middle of the breather. In addition to open channels 0 and -1 that are seen far from the breather, closed channels -3, -2, and $+1$ are visible here.

Figure 5.6: Discrete Fourier transforms of the time evolution far from the breather and in the middle of the breather for the experiment in Figure 5.4 with an incoming optical wave. The notations are the same as in Figure 5.5. See the main text for an explanation of the peaks around 4 kHz and 11 kHz.

In this discussion, we accounted for the peaks in the Fourier transform due to the incoming wave and to the interaction with the breather. However, two peaks in Figure 5.6 remain unexplained. Those two peaks are separated by approximately one breather frequency, suggesting that they are caused by the same effect and that one is due to a scattering of the other by the breather. The first peak is located near the end of the acoustic band. In the time series for site 400, we see that the beginning of the signal is responsible for this peak. Although this is before the optical wave packet reaches site 400, the time series shows clear small-amplitude oscillations at frequency 3.9 kHz. We conjecture that the propagation of the optical wave packet gives rise to an acoustic wave packet of the same wavenumber. Indeed, the dispersion relation for the wavenumber that we used ($q = \pi/3$) gives $f = 3.87$ kHz, in good agreement with the observed peak. Although this explanation seems plausible and is supported by close examination of the tail of the optical wave packet (in Figure 5.7), the precise mechanism according to which this small acoustic wave is created is unknown. This effect is independent of the size of the envelope controlled by the parameter σ.

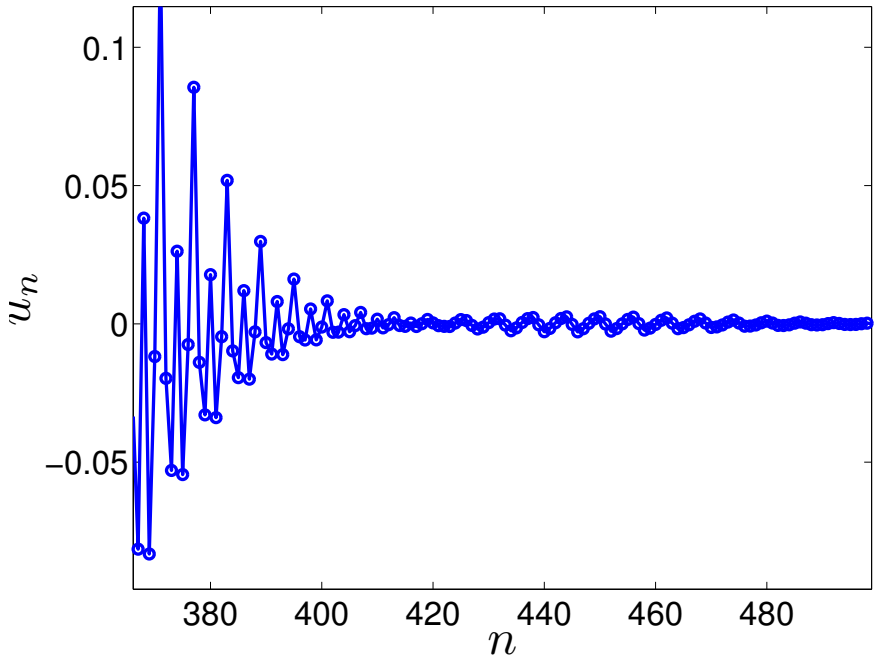

Figure 5.7: Magnification of the tail of the incoming optical wave packet of Figure 5.6, showing a secondary small-amplitude acoustic wave that propagates faster than the optical wave.

All these results confirm the validity of the theoretical approach. We now look for Fano resonances in the single-channel case. Before considering the full problem of resonances in our Hertzian chain, we examine available results for the monoatomic $K_2 - K_3 - K_4$ model, which we encountered as an approximation of our Hertz contact in Section 3.3 and where breathers were found to exist when $\frac{K_3^2}{K_2 K_4} < \frac{3}{4}$.

5.3 Fano Resonances in the $K_2 - K_3 - K_4$ Model

In 2005, Flach and Gorbach found Fano resonances in the monoatomic $K_2 - K_3 - K_4$ chain in certain parameter regimes [15]. They numerically found that the Floquet multipliers of some breathers (see Section 3.5) include small deviations from the unit circle, associated with eigenvectors representing extended states. Although we found in Section 3.5 that such oscillatory instabilities were usually connected with finite-size effects and disappeared in the limit of an infinite chain, the instabilities in this case do not depend on the size of the system. They are the signatures of a Fano resonance: an instability connected with an eigenvalue pair of complex angle $e^{i\omega_q T_b}$ is linked to a Fano resonance at frequency ω_q. We plot the breather they use in Figure 5.8.

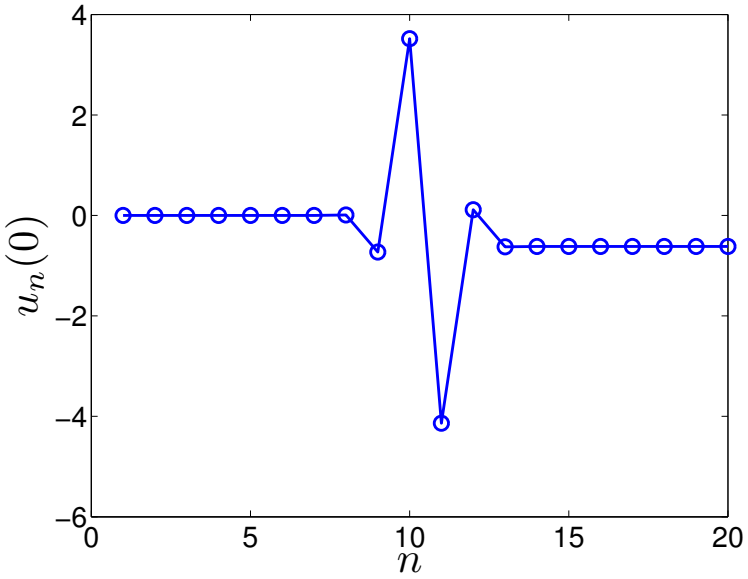

Figure 5.8: A breather in the $K_2 - K_3 - K_4$ model, with frequency $\Omega_b = 10$. The parameters are $m = 1$, $K_2 = 1$, $K_3 = 0.5$, and $K_4 = 1$.

As shown in their paper [15], there is a Fano resonance near $q = q_f \approx 2.18$, where the transmission coefficient jumps from 1 for $q \lesssim q_f$ to zero for $q \gtrsim q_f$. Correspondingly, there is a small oscillatory instability that is independent of the system size. To obtain the values of the transmission coefficient, they used a numerical method based on Newton's method to resolve a scattering state. However, I was unable to implement this method successfully. Therefore, I tried to reproduce their results by sending a Gaussian wave packet towards the breather, which is how we validated the Fano resonances in waveguide arrays and the multichannel scattering in the Hertzian chain.

We find that an interesting phenomenon does take place at $q \approx 2.18$, but the effect we observe is surprising. Instead of a nearly perfect reflection or transmission as we would expect from the transmission coefficient in Reference [15], an exponentially localised mode grows in the middle of the breather, as depicted in Figure 5.9. This mode grows exponentially in the linear regime, as shown here, but saturates when using the nonlinear equations.

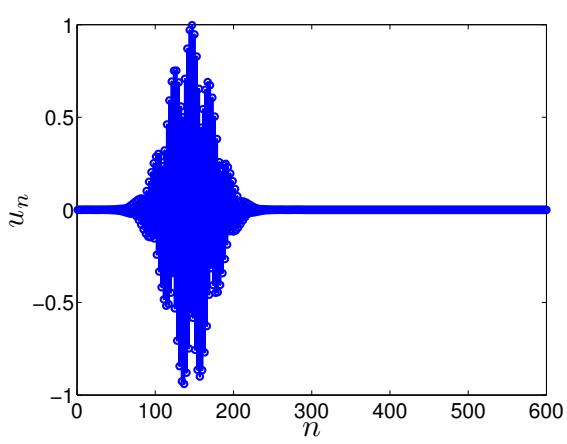

(a) Before the scattering.

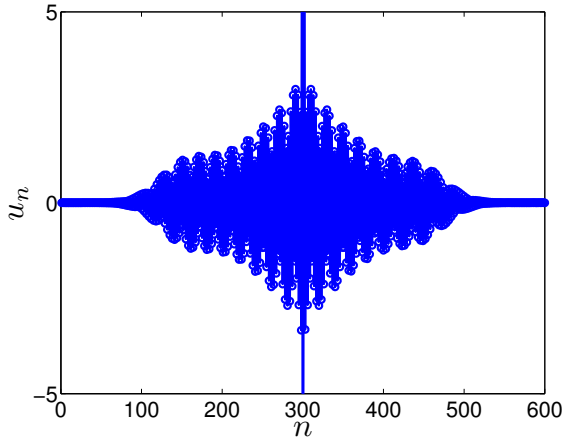

(b) After the scattering, when the reflected wave is back to its starting position.

Figure 5.9: Scattering of an incoming packet of wavenumber $q = 2.18$ by the breather shown in Figure 5.8, located at the middle of the chain at $n = 300$. These results are obtained with the linearised equations (3.10) with a chain of $N = 600$ sites. The same experiment on the nonlinear equations (2.2) shows that this phenomenon is only modified by a saturation of the exponential growth due to nonlinear effects.

In an attempt to understand this effect, we inspect the frequency content of the different sites. Far from the breather, we observe a very sharp peak at frequency ω_q, which implies that no additional frequencies were created in the scattering process. At the centre of the breather however, we observe closed channels (Figure 5.10). Two unexplained effects appear there: a frequency shift, and a point of surprisingly low amplitude.

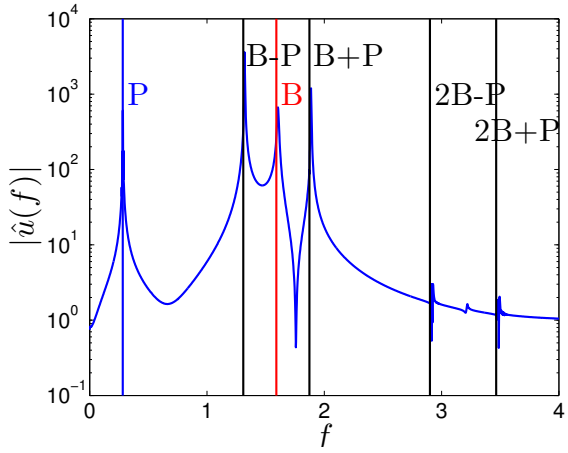

(a) Discrete Fourier transform of site $n = 300$, in the middle of the breather in the experiment of Figure 5.9

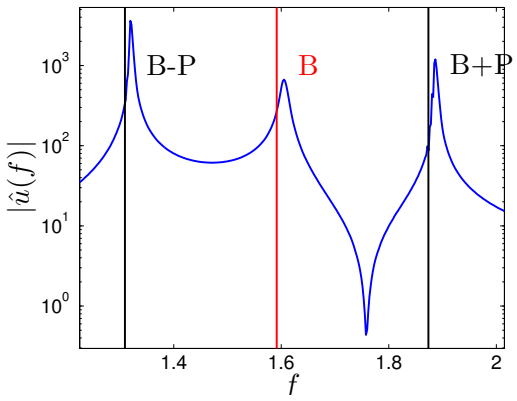

(b) Magnification of the middle part of (a).

Figure 5.10: Frequency content of site $n = 300$. Although a superficial observation of (a) suggests the usual structure of closed channels (see, for instance, Figure 5.5), close examination of (b) reveals two interesting features. First, there is a frequency shift in the breather frequency Ω_b; second, there is a dip between Ω_b and $\Omega_b + \omega_q$ that is too sharp to be a simple transition between two peaks. We do not currently have an explanation for these effects.

Another way of testing resonances is to excite the boundary of our domain with a sine wave at a particular frequency, as was used in the experiments [3]. We imposed

$$u_0(t) = 10^{-4} \sin(\omega_q t)$$

at the left boundary of the breather in Figure 5.8, and obtained the same phenomenon as with wave packets: a localised mode grows at the centre of the breather and is saturated by nonlinear effects.

It is tempting to dismiss all these effects as numerical artifacts, with no relevance to our problem, but careful examination shows that this is not the case. We consider two potential sources of errors.

First, the numerical accuracy of our integration scheme is necessarily limited. The integrations are done with MATLAB's `ode45` command, which provides an error control via two parameters `RelTol` and `AbsTol`. Performing the integration with tighter error tolerances resulted in the same effect, strongly suggesting that what we observe is not a numerical artifact.

Second, the localisation of the wave packet implies that it is not a perfect plane wave, but contains a range of frequencies. If its spectral width is larger than the frequency range over which the transition from $T = 1$ to $T = 0$ takes place, then the results will not accurately reflect the scattering for the chosen frequency. However, the wave packets that we use are more than ten times wider than the wavelength $\frac{2\pi}{q}$ and numerical experimentation with

different widths shows little sensitivity of the scattering process to the width of the wave packet, suggesting that our choice is appropriate.

Finally, this effect is very robust, and we observed them using with different breather frequencies and parameters (for instance, the resonance at $q \approx 0.62$ for a breather of frequency $\Omega_b = 4.5$ in Figure 12 of Reference [15]).

Although these results do not directly correspond to the expected mechanism of Fano resonances, they do appear where Flach and Gorbach predicted Fano resonances would take place. For instance, in the experiment of Figure 5.9, the localised mode only appears for $q \in [2.1, 2.3]$, a strong sign that it is closely related to the predicted Fano resonance at $q \approx 2.18$. Therefore, we conjecture that this mechanism is the way Fano resonances appear in this system. This suggests that the dynamics of the scattering are not adequately understood by only considering the transmission coefficient.

In this section, weconsider our original problem of Fano resonances in the Hertzian chain.

5.4 Fano Resonances in the Hertzian Chain

We explored the scattering process in our Hertzian chain for a wide range of wavenumbers and breather frequencies in the Hertzian chain, using the method of wavepackets previously described. We did not find any phenomenon comparable to Fano resonances or the growth of a local mode we discussed in the $K_2 - K_3 - K_4$ model. Rather, we observe different forms of multi-channel scattering and simple transmission with no signs of resonances.

A possibility remains that Fano resonances exist for other parameter values of our model. Recalling the evolution equation

$$m_n \ddot{u}_n = A\left[\Delta - (u_n - u_{n-1})\right]_+^{3/2} - A\left[\Delta - (u_{n+1} - u_n)\right]_+^{3/2},$$

using the substitution $u_n = \Delta u'_n$, $t = \sqrt{\frac{\sqrt{\Delta} m_1}{A}} t'$ and dropping the primes, we obtain

$$m_n \ddot{u}_n = \left[1 - (u_n - u_{n-1})\right]_+^{3/2} - \left[1 - (u_{n+1} - u_n)\right]_+^{3/2},$$

where $m_n = 1$ if n is odd, and m_2/m_1 if n is even. Therefore, we conclude that the only model parameter that can affect the scattering process is the mass ratio m_2/m_1: both A and Δ can be scaled away. We explored wave scattering with different values of this mass ratio (although an exhaustive study is out of reach of our numerical methods), each time sampling all available wavenumbers and breather frequencies, again finding no trace of Fano resonances. Therefore, we conjecture that no Fano resonances are present in the Hertzian chain.

These scattering results and breather properties (in particular, their stability) were checked to hold in the $K_2 - K_3 - K_4$ approximation to our Hertz potential given by (3.6). Although this modified model results in a small change in breathers amplitudes and profiles, the properties are mostly the same. In particular, no resonances were found in this reduced model. Assuming that all of the scattering properties of the Hertzian chain are preserved in the $K_2 - K_3 - K_4$ approximation, the diatomic Hertzian chain can be seen as a particular

instance of the diatomic $K_2 - K_3 - K_4$ model, with Equations (3.6) defining a subspace of the parameter space (K_2, K_3, K_4). We conjecture that the Fano resonances found for $m_1 = m_2 = 1, K_2 = 1, K_3 = 0.5$, and $K_4 = 1$ are unavailable to the reduced parameter space defined by the diatomic Hertzian chain. This conjecture could be verified by following the Fano resonances when the parameters are varied and find exactly where they are lost. In particular, if an uninterrupted branch of breathers could be continued from the model used by Flach (the monoatomic $K_2 - K_3 - K_4$ chain with $m_1 = m_2 = 1, K_2 = 1$, $K_3 = 0.5$, and $K_4 = 1$) to the model we use (the diatomic $K_2 - K_3 - K_4$ with parameters dictated by (3.6)), then we could perform a (numerical) bifurcation analysis explaining when and why Fano resonances are lost.

In conclusion, although we cannot completely rule out the possibility of Fano resonances in the Hertzian chain, the results we obtained seem to point to the nonexistence of such resonances. Even if they exist, direct simulation of the equations of motion shows that their observation is problematic, as explained in the previous section. Therefore, an experimental observation of a Fano resonance in granular chains seems unlikely.

6 Conclusions

In this report, we introduced the equation used to model chains of solid beads. After examining properties of linear and solitary waves, we focused on localised excitations, called breathers. We studied their existence and stability, and used numerical methods to obtain them to high accuracy. We then introduced the concept of Fano resonances in progressively more complicated examples, before presenting the results of Reference [31], a theoretical derivation and numerical confirmation of a Fano resonance in a model of waveguide arrays. Although our original goal was to extend these results to breather in Hertzian chains, we illustrated on the example of the $K_2 - K_3 - K_4$ model, for which Fano resonances were predicted in Reference [15], that the direct use of the numerical method developed for the waveguide arrays is problematic. We uncovered an interesting phenomenon that needs to be studied in greater detail to have any hope of finding Fano resonances in more complicated systems such as the Hertzian chain.

During this study, we coded several numerical methods. The fine-tuning of parameters (such as the various accuracy settings) had to be done manually in each case, and the various settings interacted in complex ways. This would benefit from a more systematic study. For instance, given a differential equation that is integrated with specified absolute and relative tolerances at each timestep, what are the resulting error bounds, and how should we choose the various parameters of a Newton's method using this differential equation as objective function, as we did to obtain breathers? Which variants of Newton's method are appropriate to extend the convergence region or improve the computation time? (For instance, we used Broyden's method [4] to avoid recomputing the Jacobian matrix at each step) Should the Jacobian be computed by finite differences or by integration of the linearised equations? In both cases, because the Jacobian is numerically sparse, we could have used a collocation method [9] or even automatic differentiation [21]. Also, the continuation procedure we

used is very crude and does not adequately detect bifurcation (since the Jacobian becomes singular). A very promising option is to use a package such as AUTO [10] to follow branches of solutions.

Although some results were reported in Reference [39] about the various breathers supported by Hertzian chains, an interesting and ambitious goal would be to establish an exhaustive classification of all breather branches, and link them to relevant limiting cases by numerical continuation. Also interesting would be the study of breathers in chains of beads with different contact geometries, *i.e.* different exponents in the contact law (for instance, $F = \delta^2$ for conical asperities [20]). Future areas of research also include higher-dimensional lattices and accounting for energy dissipation, an important issue for experimental studies [5].

Concerning Fano resonances, we found in Section 5.3 that an important issue to be addressed is the study of scattering by discrete breathers in the presence of Fano resonances, going beyond the classical approach of computing scattering states and transmission coefficients. We conjectured the nonexistence of Fano resonances in the Hertzian chain, and outlined a plan to confirm this using a bifurcation analysis.

Our results also suggest possible future experiments. For instance, we can already recommend the observation of multichannel scattering. If a long-lived breather can be created, then using a sine wave of a well-chosen frequency in the acoustic band as input voltage of the actuator should result in the observable creation of an optical wave (see Figure 5.2) by the breather. However, the experimental observation of Fano resonances does not seem to be a likely outcome, because of the uncertainty of their existence in our parameter regime mentioned in Section 5.4 and the difficulty of their observation studied in Section 5.3.

References

[1] E. L. Allgower and K. Georg. *Introduction to Numerical Continuation Methods*. Society for Industrial and Applied Mathematics, Philadelphia, PA, USA, 2003.

[2] H. Beutler. Über Absorptionsserien von Argon, Krypton und Xenon in Termen zwischen den beiden Ionisierungsgrenzen $^2P_3^{2/0}$ und $^2P_1^{2/0}$. *Z. Phys. A*, 93:177–196, 1935.

[3] N. Boechler, G. Theocharis, S. Job, P. G. Kevrekidis, M. A. Porter, and C. Daraio. Discrete breathers in one-dimensional diatomic granular crystals. *Phys. Rev. Lett.*, 104(24):244302, 2010.

[4] C. Broyden. A class of methods for solving nonlinear simultaneous equations. *Mathematics of Computation*, 19:577–593, 1965.

[5] R. Carretero-González, D. Khatri, M. A. Porter, P. G. Kevrekidis, and C. Daraio. Dissipative solitary waves in granular crystals. *Phys. Rev. Lett.*, 102(2):024102, 2009.

[6] A. Chatterjee. Asymptotic solution for solitary waves in a chain of elastic spheres. *Phys. Rev. E*, 59(5):5912–5919, 1999.

[7] D. Chen, S. Aubry, and G. P. Tsironis. Breather mobility in discrete φ^4 nonlinear lattices. *Phys. Rev. Lett.*, 77(23):4776–4779, 1996.

[8] C. Coste, E. Falcon, and S. Fauve. Solitary waves in a chain of beads under hertz contact. *Phys. Rev. E*, 56(5):6104–6117, 1997.

[9] A. R. Curtis, M. J. D. Powell, and J. K. Reid. On the Estimation of Sparse Jacobian Matrices. *IMA J Appl Math*, 13(1):117–119, 1974.

[10] E. J. Doedel, A. R. Champneys, T. F. Fairgrieve, Y. A. Kuznetsov, B. Sandstede, and X. Wang. AUTO 97: Continuation and bifurcation software for ordinary differential equations.

[11] E. Falcon. *Comportements dynamiques associés au contact de Hertz : processus collectifs de collision et propagation d'ondes solitaires dans les milieux granulaires.* PhD thesis, Université Claude Bernard Lyon I, 1997.

[12] U. Fano. Effects of configuration interaction on intensities and phase shifts. *Physical Review*, 124(6):1866–1878, 1961.

[13] E. Fermi, J. Pasta, and S. Ulam. Studies of nonlinear problems i. *Los Alamos report LA-1940*, 1955.

[14] S. Flach. Conditions on the existence of localized excitations in nonlinear discrete systems. *Phys. Rev. E*, 50(4):3134–3142, 1994.

[15] S. Flach and A. Gorbach. Discrete breathers in Fermi-Pasta-Ulam lattices. *Chaos*, 15(1):1–10, 2005.

[16] S. Flach and A. V. Gorbach. Discrete breathers – advances in theory and applications. *Physics Reports*, 467(1-3):1 – 116, 2008.

[17] S. Flach, A. E. Miroshnichenko, and M. V. Fistul. Wave scattering by discrete breathers. *Chaos*, 13(2):596–609, 2003.

[18] F. Flicker. Nonlinear waves in granular crystals. Master's thesis, MPhys, University of Oxford, 2010. Available at `http://people.maths.ox.ac.uk/porterm/felix_report_final.pdf`.

[19] G. Friesecke and J. Wattis. Existence theorem for solitary waves on lattices. *Commun. Math. Phys.*, 161(2):391 – 418, 1994.

[20] G. Fu. An extension of Hertz's theory in contact mechanics. *Journal of Applied Mechanics*, 74(2):373–374, 2007.

[21] A. Griewank and G. Corliss. *Automatic Differentiation of Algorithms: Theory, Implementation, and Application.* Society for Industrial and Applied Mathematics, Philadelphia, PA, USA, 1992.

[22] G. Huang and B. Hu. Asymmetric gap soliton modes in diatomic lattices with cubic and quartic nonlinearity. *Phys. Rev. B*, 57(10):5746–5757, 1998.

[23] K. L. Johnson. *Contact Mechanics*. Cambridge University Press, 1987.

[24] C. Kittel. *Introduction to Solid State Physics*. Wiley, 7th edition, 1995.

[25] S. G. Krantz and H. R. Parks. *The Implicit Function Theorem : History, Theory, and Applications*. Boston, EUA : Birkhäuser, 2002.

[26] R. S. Mackay and S. Aubry. Proof of existence of breathers for time-reversible or Hamiltonian networks of weakly coupled oscillators. *Nonlinearity*, 7(6):1623–1643, 1994.

[27] J. L. Marín and S. Aubry. Breathers in nonlinear lattices: numerical calculation from the anticontinuous limit. *Nonlinearity*, 9(6):1501, 1996.

[28] J. L. Marín and S. Aubry. Finite size effects on instabilities of discrete breathers. *Physica D: Nonlinear Phenomena*, 119(1-2):163 – 174, 1998.

[29] A. E. Miroshnichenko, S. Flach, and Y. S. Kivshar. Fano resonances in nanoscale structures. *ArXiv 0902.3014*, 2009.

[30] A. E. Miroshnichenko, S. F. Mingaleev, S. Flach, and Y. S. Kivshar. Nonlinear Fano resonance and bistable wave transmission. *Phys. Rev. E*, 71(3):036626, 2005.

[31] U. Naether, D. E. Rivas, M. A. Larenas, M. I. Molina, and R. A. Vicencio. Fano resonances in waveguide arrays with saturable nonlinearity. *Opt. Lett.*, 34(18):2721–2723, 2009.

[32] V. Nesterenko. *Dynamics of Heterogeneous Materials*. Springer, New York, 2001.

[33] V. Nesterenko. Propagation of nonlinear compression pulses in granular media. *J. Appl. Mech. Tech. Phys.*, 24(5):733 – 743, 1983. Translated from *Zhurnal Prikladnoi Mekhaniki i Tekhnicheskoi Fiziki*, 5: 136-148, 1983.

[34] A. A. Ovchinnikov. Localized Long-lived Vibrational States in Molecular Crystals. *Soviet Journal of Experimental and Theoretical Physics*, 30:147, 1969.

[35] M. A. Porter, N. J. Zabusky, B. Hu, and D. K. Campbell. Fermi, Pasta, Ulam and the birth of experimental mathematics. *American Scientist*, 97(6):214–222, 2009.

[36] M. Porter, C. Daraio, I. Szelengowicz, E. Herbold, and P. Kevrekidis. Highly nonlinear solitary waves in heterogeneous periodic granular media. *Physica D: Nonlinear Phenomena*, 238(6):666–676, 2009.

[37] W. H. Press, S. A. Teukolsky, W. T. Vetterling, and B. P. Flannery. *Numerical Recipes: The Art of Scientific Computing*. Cambridge University Press, 3rd edition, 2007.

[38] S. Sen, J. Hong, J. Bang, E. Avalos, and R. Doney. Solitary waves in the granular chain. *Physics Reports*, 462(2):21 – 66, 2008.

[39] G. Theocharis, P. G. Kevrekidis, N. Boechler, S. Job, M. A. Porter, and C. Daraio. Discrete gap breathers in one-dimensional diatomic granular crystals. *In preparation*, 2010.

[40] S. J. Yong, M. S. Arkady, and S. K. Chang. Classical analogy of Fano resonances. *Physica Scripta*, 74(2):259, 2006.